

Optical Biosensors

Second Semester Report
Spring Semester 2008

by

Allan Fierro
David Sehrt
Doug Trujillo
Evan Vlcek
Michael Bretz

Prepared to partially fulfill the requirements for
ECE402

Department of Electrical and Computer Engineering
Colorado State University
Fort Collins, Colorado 80523

Report Approved: _____

Project Advisor

Senior Design Coordinator

ABSTRACT

Currently cell sorting is both an expensive and arduous task. Optofluidic Intracavity Spectroscopy (OFIS) is a low-cost, attractive alternative to these other cell sorting methods such as flow cytometry. Unlike flow cytometry, OFIS doesn't contaminate the samples with fluorescent tagging. OFIS relies instead on index of refraction of the cells, which allows for observation of these cells in their natural state. The current procedure for OFIS demands an observer to monitor cells flowing through a microfluidic channel, trap a cell, and set up a spectrometer reading. This demands valuable time of the observer and makes cell differentiation unnecessarily slow. In order to improve the speed of OFIS, an automation system must be implemented to detect cells, trap them, and take a measurement. To achieve acceptable speed through OFIS new hardware was engineered which includes new fabrication techniques for making the polydimethylsiloxane PDMS/glass chips with micro-fluidic channels with dielectrophoretic (DEP) traps, flow control, a detection circuit with a high gain transimpedance amplifier, a RF switch and Labview software to control the system. Each of these components required innovative thinking to improve cell differentiation with OFIS.

TABLE OF CONTENTS

I: Introduction	3
II: Channel Fabrication	5
III: DEP Chip Micro-Fluidic Ports	8
IV: Flow Control	10
V: Detection Circuit	13
VI: RF Switching.	18
VII: DEP Trapping	18
VIII: Future Work	15
References	22
Appendix A – Abbreviations	23
Appendix B – Budget	23
Appendix C – Peripherals	24
Appendix D – Project Tips and Tricks	34
Appendix E – Data Sheets and User Manuals	39
Acknowledgements	57

FIGURES

Figure 2.1	5
Figure 2.2	7
Figure 3.1	8
Figure 3.2	9
Figure 4	11
Figure 5.1	13
Figure 5.2	13
Figure 5.3	14
Figure 5.4	15
Figure 5.5	16
Figure 5.6	16
Figure 5.7	16
Figure 5.8	16
Figure 6.1	20
Figure 6.2	21
Figure C1.1	25
Figure C1.2	26

Figure C1.3	27
Figure C2.1	30
Figure C2.2	31
Figure C2.3	31
Figure C2.4	32
Figure C2.5	33
Figure E2.1	36
Figure E2.2	38

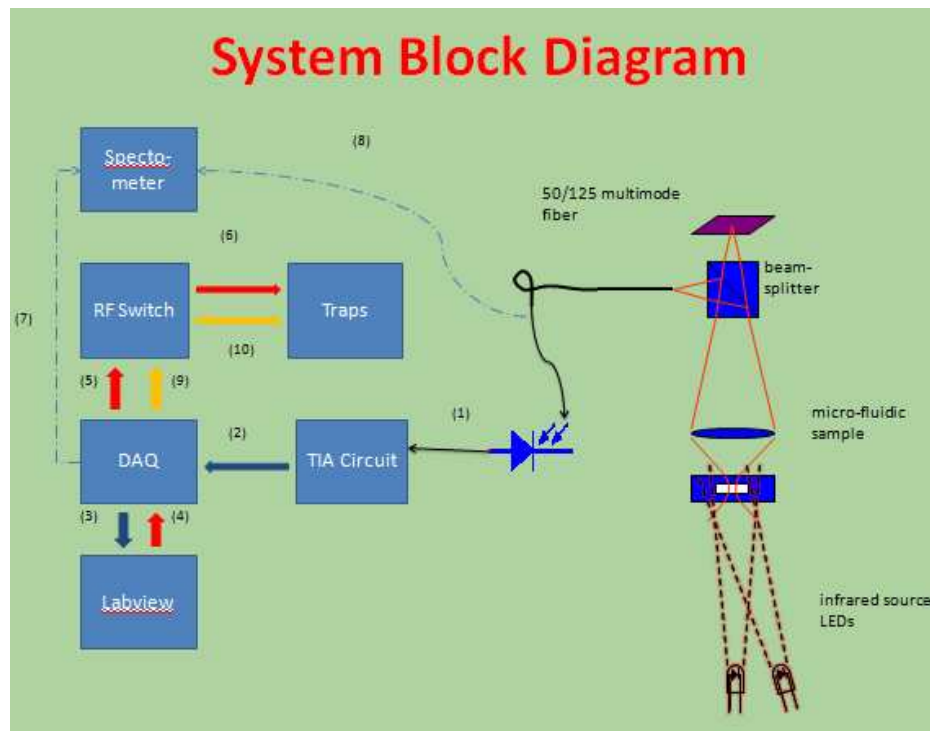
Chapter I: Introduction

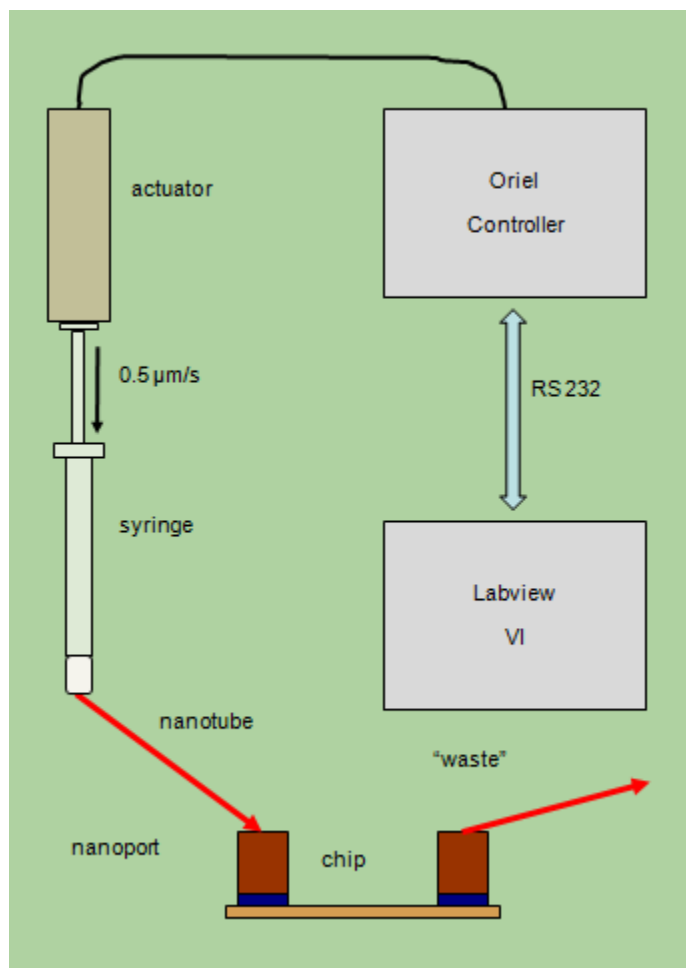
As of right now, the main procedure for distinguishing cells apart is flow cytometry. We are working on a more cost efficient method called optofluidic intracavity spectroscopy (OFIS). This procedure has the advantage of not using fluorescent tags, which are quite expensive and add to the time needed for the sample preparation. By using the refraction of light through the cells instead of fluorescents we can observe the cells in a more natural, or pure, form and therefore do not have to worry about the chance that the tags may interfere with normal cell function.

The components of our system are: a microscope, an infrared LED, a cell detection circuit, a data acquisition unit with analog to digital convertor and digital output, computer control software, a function generator, a RF switch, a DEP chip with the micro-fluidic channel in it, and a spectrometer. (See figures below) To date, we have made a channel to flow our sample solution through. This channel has metal leads (DEP traps) for setting up the electric field to trap our cell when it is detected by the detection circuit to be analyzed by the spectrometer. We first had to build the channels with the traps on them. The next step was to determine the proper flow rate of the solution so as to optimize trapping. We also made a circuit to detect the presence of a cell to trigger the trap. All of the control was done with Labview software.

The way our system works is as follows. First, light from an infrared light emitting diode (IR LED) wavelength peak centered at 850nm is focused through the cavity of the micro-fluidic channel on the chip. The light passes through up to the microscope and out from the microscope via a fiber optical cable into our detection circuit. This light gets converted into a current in the nA range using a photodiode and then goes into a transimpedance amplifier to get converted to a voltage and to be amplified. This voltage is sent to a data acquisition device (DAQ) to compare the voltage with a preset reference voltage. If the input voltage is below the preset value the DAQ will send a signal to close the RF switch in order to send a 6 or 10 MHz 10 Vpp signal to the DEP traps on the chip. This will stop and hold a cell in the trap for analyses by the spectrometer to distinguish the cell. In order for the DEP trap to be able to capture a cell the

sample solution must be flowing at a slow enough rate so as to not have the cells have too much inertia. This is done by using a micro-pump and software (Labview) to create a pulse width modulation to have the proper duty cycle to get the flow rate we need.





Chapter 2 will discuss the fabrication of our chips and how the channels are made and how the traps and leads are added to the chip. Chapter 3 will be on DEP chip micro-fluidic ports. Chapter 4 will discuss the flow control of the microfluidics we used plus the pump system. Chapter 5 will discuss the detection circuit we designed and some of the components used. Chapter 6 will discuss DEP trapping. Chapter 7 will cover the future work and recommendations for next year.

Chapter II: Channel Fabrication

Photolithography was used to fabricate these dielectrophoretic traps in the CSU Cleanroom. This process allows building contacts, wires, and effectively traps on a micron scale. The DEP chips were built with two distinct components, a DEP trapping circuit and a microfluidic channel. These two components are bonded together to form a DEP trap.

The DEP trapping circuit is composed of three contacts and three discrete lines running through the area under the channel. The conductive material used was gold and chrome. These

metals were first deposited onto a glass slide using an evaporator in the cleanroom. A layer 30nm thick of chrome was first deposited onto the slide. This thin layer of chrome is deposited because chrome can adhere to glass much better than gold can. A 120nm layer of gold is then placed over the chrome layer. Gold is deposited because of its low resistance and low chemical reactivity. Once this deposition is completed, photolithography follows. AZ1512 Photoresist is placed and then spun on the chip. This resist is thinner and has very good resolution. A soft bake at 110 degrees Celsius for 1 minute follows. Next the chrome DEP mask is used to pattern the resist. A chrome mask is chosen for this exposure because of the small features it encompasses. Chrome masks are expensive, about \$400 for a 3 μm resolution 4"x4" plate, but have a high resolution and have an antireflective coating to enhance the exposure. This mask contains patterns for two different trapping circuits to select from. A characterization of the AZ1512 resist found an exposure time with the soft bake of 10 seconds. The resist is exposed for 10 seconds which maximizes the resolution of the resist. The exposed resist is then developed leaving the unexposed area covered. A two step wet etch removes the uncovered gold and chrome from the glass slide. The DEP trap chip is then ready for two of the three types of bonding. The DEP channels were composed of either polydimethylsiloxane (PDMS) or glass. PDMS channels were the majority of the channels prepared since the fabrication success rate of these channels was much higher than glass. The success of PDMS is attributed to its exceptional adherence to glass. The PDMS used was made of bulk PDMS and the PDMS curing agent with a mass ratio of 10:1 respectively. This PDMS is then placed in a vacuum and degassed. Degassing will remove the impurities in the PDMS which will improve the optical properties of the molded part. A mold of the channel was needed to form the channel. This mold is composed of a silicon substrate and SU-8 resist. This epoxy based resist is much thicker and viscous than the AZ1512 and can be used as a mold when it is baked and fully developed. Once the mold is constructed PDMS solution is poured into the mold again degassed. Once degassed the mold is placed in an oven to bake for at least 4 hours. The curing agent transforms this viscous liquid into an elastic solid. The PDMS can then be cut and peeled off the silicon substrate. A glass cover slip is then placed on the opposite side of the channel which keeps the PDMS chip clean and allows the channel to be transported easier. In order for the PDMS channel to be bonded to the DEP trapping circuit one more step in the DEP circuit must be performed. A gold and chrome sheet still remains outside of the trapping circuit which is used for other bonding processes. This area is removed with the same lithography steps as creating the traps except that a mask covering the trapping circuit is used. Now the two chips are ready to be bonded together. The DEP chip is taped to a glass slide with the circuit facing out. Both chips are then oxygen-plasma treated with a micro-RIE. After treatment the two chips are bonded together using the mask aligner. The PDMS channel is placed on the stage facing up. The DEP chip is positioned facing down being held in the mask holder. The DEP traps are then positioned over the channel. The

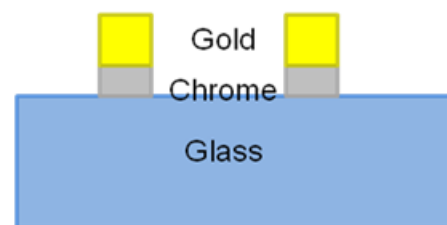


Figure 2.1

channel is then brought into contact with the DEP circuit chip. The two are now bonded together. The mask holder is then unscrewed and pulled out vertically from the aligner.

Glass channels were experimented with as well. These glass channels are more desirable than PDMS because a dielectric coating can be deposited on the surface of glass producing an optical cavity necessary for cell differentiation. Pyrex glass is used for channel etching and chrome and gold are deposited on the surface. A thick layer of P4400 positive resist is deposited onto the surface. This resist was chosen because it is much thicker than the AZ1512 resist which will be necessary with HF etching. The tradeoff with using P4400 is that it doesn't have as good a resolution as AZ1512. In this application giving up resolution is certainly acceptable. The soft bake for this resist is 110 degrees Celsius for 2 minutes. The resist is then exposed with the channel mask for 35 seconds. The exposed area is washed away in development. The chip is then baked at 110 degrees Celsius for 10 minutes. This turns the resist into a hard film which can withstand the wet etching process. The gold and chrome are etched away. The next step is to etch the glass. This is done using a wet etch of HF. The chip is placed in HF for approximately 3-4 minutes. The chip is removed from the HF and washed with de-ionized water. The chip is then placed in an acetone bath to remove the hardened resist. Acceptable glass etching was never achieved in the semester. The channel surface must be as uniform as possible to provide better transmission of light. Using an Alpha Step surface profilometer to measure the surface height, deep indents were found in the glass. One explanation to this result is that there are lattice impurities in the glass that etch faster than the uniform lattice. If this were the case then higher quality glass would be needed to perform suitable glass etching.

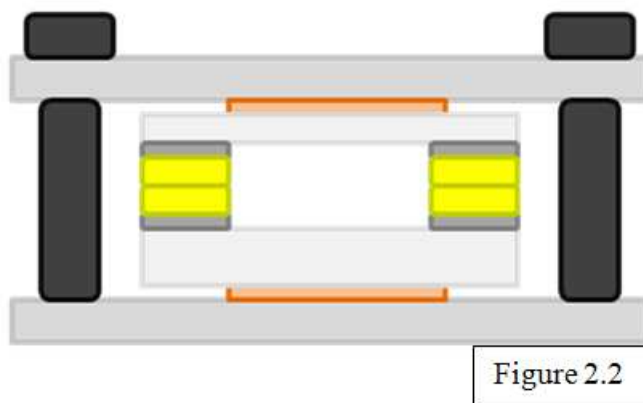


Figure 2.2

Once the layer of resist is removed, the channel chip can be bonded to the DEP trapping circuit chip. Two bonding methods have been implemented. The more successful method is Indium bonding. A piece of Indium metal and the channel with gold on the outer area are placed in a solution. A positive voltage is applied to the Indium metal and a negative voltage is placed on the of the channel chip. This creates a current of Indium to be deposited on the gold. The channel chip is then ready to bond to the DEP circuit chip. The two pieces are roughly aligned by eye and pressed together by hand. The chips are then observed under a microscope to view the alignment. Fine adjustments are made to optimize the alignment. Once the alignment is made the two chips are sandwiched between two copper sheets. These sheets are then put in a vise. The vise is screwed together with four screws. This puts equal pressure on the bonding area. The bonding vise is then placed into a heater. A vacuum is pulled in the heater to prevent

oxidation from the high temperatures. The temperature in the heater is controlled by a programmable unit attached to the heater. The temperature is then programmed to ramp up to and hold at a certain temperature and then ramp down. Once the desired temperature program completes, the bonding vice is pulled from the heater. The channel and the DEP trapping circuit chips are now bonded together.

A similar bonding procedure is gold to gold bonding. The advantage gold has over Indium is that the height of the material required for bonding is minimal compared to Indium. Minimizing the height for bonding is critical because the height dictates how leaky the channel will become. Indium bonding adds another layer in the bonding area outside of the chip. This layer adds an additional height on the scale of microns. This will produce a leakier channel than chips bonded with a gold to gold method. This gold to gold method has not successfully been completed on test chips. These test chips are half the size of the DEP trapping circuit chips and have gold with no patterning. The two gold chips are pressed together and put between the copper plates and into the vice. The temperature is programmed to be much higher than indium bonding. This is due to the fact that Indium bonds much easier to surfaces than gold does to gold or any other surface. The melting point of gold is also very high. In order to fuse the two pieces together a very high temperature must be obtained. An appropriate temperature and pressure have not been obtained which prevent acceptable bonding. Small bonding areas have been obtained but not large enough to be a reliable method for chip bonding.

Given the difficulty of metal bonding, alternative approaches were explored but have not yet been incorporated in actual micro-fluidic channels.

Chapter III: DEP Chip Micro-Fluidic Ports

In order to get cells into the DEP chip with a micro-channel, there must be a way for cells to physically enter the chip. It is also important that there is a way for the cells to exit the chip. This is accomplished through the use of nanoports. There are two nanoports on every chip, one for the cells to enter into the channel, and one for cells to exit the channel. Nanoports are cylindrical shaped parts that are on the order of 1 – 2 cm in diameter and 2 – 3 cm tall. They are composed of a plastic-like material. On the bottom of the nanoports, there is a small circular opening with a rubber seal surrounding it. From the top, nanoports are hollow with threads so that a nanotube can be secured into the nanoport using a hollow screw-like adapter. These adapters are included as a kit when nanoports are purchased. Nanotubes are very small tubing that are 150 μm in inner diameter that are frequently used in micro-fluidics. The figure shows the basic structure of a nanoport.

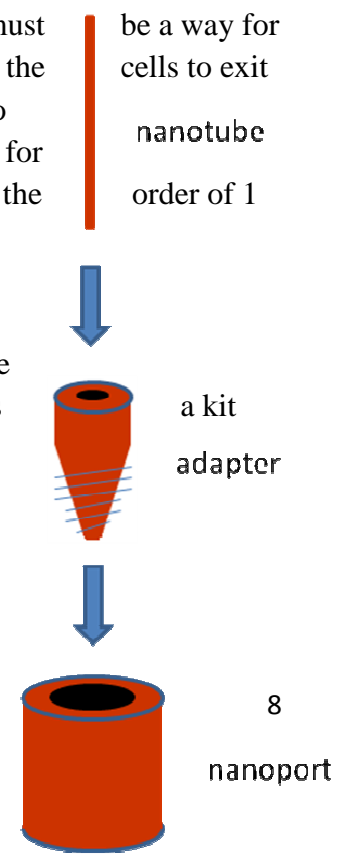


Figure 3.1: Nanotube-Nanopore Interface

Before nanopores can be placed on a chip, holes must be drilled into the chip in the appropriate places. To do this, a pattern of the chip fabrication is placed over the chip and the two places for holes are marked. Then a drill press is used with a small drill bit. Great care must be taken when drilling the holes because glass cracks and chips very easily. Water is applied at the drill area and only very small depths are drilled at a time. This process is very dependent on minimal human error. Many of the fabricated chips have non-ideal holes when drilling is complete.

It is also very important to have a way to securely place the nanopores on the DEP chip so that there is no leakage as cells and liquids are pushed into the channel and pulled back out of the channel, sometimes under high pressure. The nanopore attachment process is quite simple and never fails no matter how dirty the sample is, even for the non-adhesive type described below. Adhesive o rings are used to create the bond between the nanopore and the chip. Adhesive o rings are a sticky, glue-like material in an “O” shape that act as double-sided tape. These rings are very carefully placed around the center of the drilled holes, and pressed firmly into place. After this, the nanopores are cautiously placed on the adhesive o rings, making sure to center the nanopore over the hole. Again, this is pressed firmly into place. Once complete, the chip is clamped to the nanopore for one hour to allow the adhesive o ring to dry and seal. The figure below shows the placement of a nanopore.

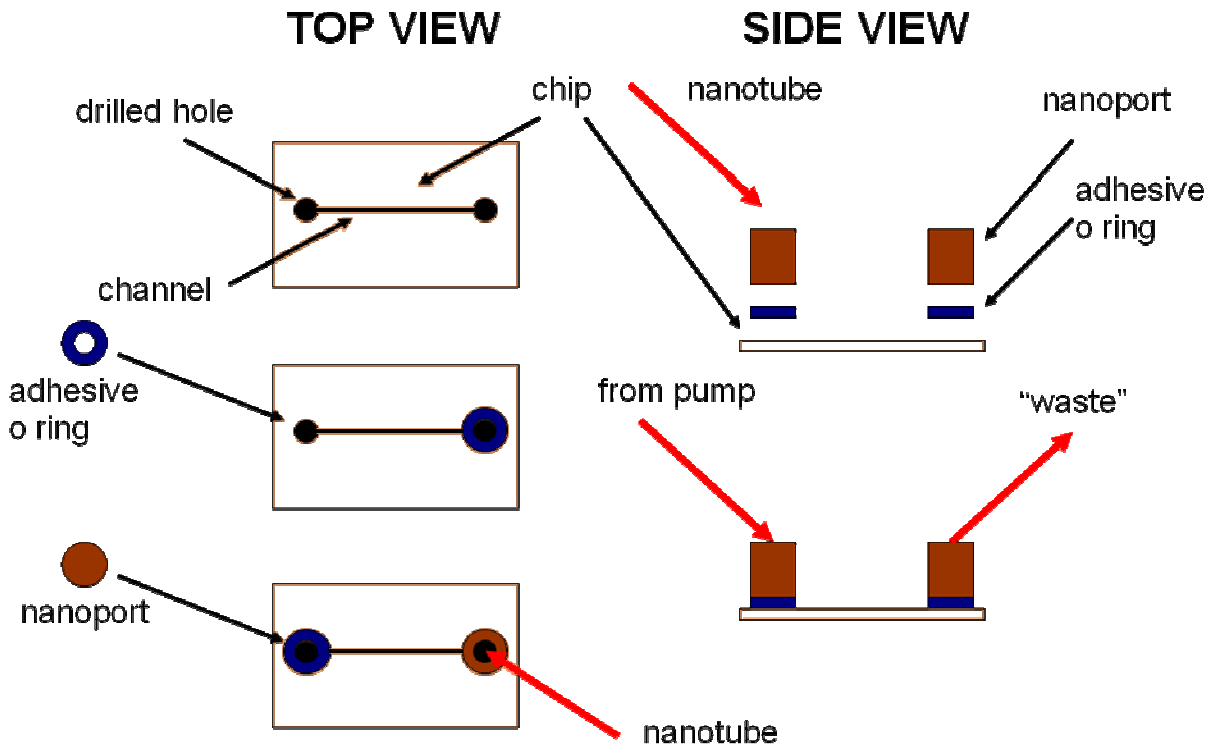


Figure 3.2: Nanopore Attachment

Second Semester Updates

The company that made the adhesive o rings no longer produces them. Their replacement o rings are non-sticky and bond via heat. The process for attaching a nanopore is nearly identical; however the final step is to bake the chip in 170°C for 1 hour. Placing the o ring and nanopore is much more difficult because the new o ring is not sticky. The bonding strength of the new o ring is very dependent on the cleanliness of the surfaces that are being bonded. A detailed description of the process of attaching the new nanopores is in Appendix E.

Chapter IV: Flow Control

An essential part of the project is to be able to get cells into the chip. There are several considerations for acceptable means to accomplish the desired flow rate of cells in the channel of the chip. The first and primary requirement is that the flow rate must be less than or equal to 40 $\mu\text{m/s}$. This requirement comes from the DEP traps on the chip. If the flow rate exceeds 40 $\mu\text{m/s}$ the force of the DEP trap to stop a cell will not be sufficient to stop a cell and hold it in place. Another limitation of flow control is that there must not be too much

pressure on the nanoport-chip seal or in the channel. The bonding on glass to glass chips is not very strong and high micro-fluidic pressure will cause the chip to leak. If leaking is severe, it is possible for cells to flow outside of the channel. Obviously, this is very undesirable because all of the traps and optical detection are near the center of the channel. It is also worth noting that all of the glass chips have gaps between the two pieces of glass due to an imperfect bonding process. This creates flow outside of the channel and different fluid dynamics than the PDMS chips. Because the glass to glass chips (glass chips) essentially have larger channels, the flow rate is significantly slower than in the PDMS chips when the same amount of pressure is applied to the fluid.

Most cell samples, such as blood, are obtained using a syringe. Therefore, a syringe is used to push samples into a nanotube and into the channel. Although the end goal of the project is to pump cells through the channel and analyze them, it is impractical to actually use cell samples to develop and test flow control. Therefore, de-ionized water was used with glass spheres ranging from 5 μm to 26 μm in diameter. The majority of the time 9.77 μm spheres were used. This water with glass spheres will be referred to as “fluid” in parts of this section. When the project first began, it was thought that the rate at which the end of a syringe plunger needed to be pushed could be calculated based on the fact that the volume in is the same as the volume out. Ideally, chips are fabricated with a 200 μm wide by 25 μm deep channel. This gives an ideal cross-sectional area of $200\ \mu\text{m} \times 25\ \mu\text{m} = 5000\ \mu\text{m}^2$. If the syringe plunger is pushed at a rate of $x\ \mu\text{m/s}$ then the volume of fluid flowing into the nanotube (and the chip) is $\pi \times (0.5 \times \text{diameter of syringe } [\mu\text{m}])^2 \times x\ \mu\text{m/s} = z\ \mu\text{m}^3/\text{s}$. This flow rate must logically be the same in the channel since the volume in must equal the volume out. This result can then be used to calculate the velocity at which fluid will travel through the channel. The equation is as follows: $v\ \mu\text{m/s} = z\ \mu\text{m}^3/\text{s} \times (5000\ \mu\text{m}^2)^{-1}$. Substituting the first equation into the second gives a direct relationship between the velocity of fluid in the channel $v\ [\mu\text{m/s}]$ and the velocity at which the plunger of the syringe is pushed $x\ [\mu\text{m/s}]$. This resulting equation is:

$$v\ \mu\text{m/s} = x\ \mu\text{m/s} \times \pi \times (0.5 \times \text{diameter of syringe } [\mu\text{m}])^2 \times (5000\ \mu\text{m}^2)^{-1}$$

The only syringes on hand at the beginning of the project were 3 cc syringes with a diameter of 8.585 mm = 8585 μm manufactured by B-D. Using the equation above equation, to achieve a 40 $\mu\text{m/s}$ flow rate in the channel, the plunger must be pushed at a rate of 0.00346 $\mu\text{m/s}$. The original plan for flow control was an industrial syringe pump. Borrowed from the chemistry department, the NE – 1000 syringe pump made by New Era Pump Systems, Inc. can push this B-D syringe at a rate of 2.434 $\mu\text{L/hr}$. This is the equivalent of $6.761 \times 10^5\ \mu\text{m/s}$. This is 1.954×10^8 times too fast! Obviously this syringe pump is not a valid solution to the flow rate problem. In addition, when the syringe pump was set to its slowest setting, the torque broke the encoder coupler because the pressure in the chip created a force pushing back against the syringe plunger that was beyond what the pump was designed for.

As a solution, the Oriel Instruments Encoder Mike Controller 18011 was chosen to function as a custom pump. The Oriel Instruments Encoder Mike Controller 18011 (Oriel) is designed to be used as a precise way to move a microscope stage. It can move the actuator at a minimum velocity of 0.5 μm , which is still about 150 times faster than the desired rate for the larger syringe (8.585 mm diameter). To reduce the rate at which the plunger must move, a

smaller syringe (4.669 mm diameter) was chosen to be used in the system. This syringe plunger only needs to move at a rate of $0.0115 \mu\text{m/s}$ to achieve the desired flow rate of $40 \mu\text{m/s}$ in the channel. Because this is still slower than what the Oriel is capable of, Labview software was used to create a duty cycle where the actuator is only moving for a small percentage of the time. For details on how the Oriel was implemented into the system, see Appendix C2. To achieve $40 \mu\text{m/s}$ velocity inside the channel, the Labview VI was set so that the actuator moved for 0.825 seconds at $0.5 \mu\text{m/s}$ ($0.4125 \mu\text{m}$) and off for 7 seconds. When the VI is used, the optimal flow rate occurs at this duty cycle of approximately 10.5%. This “duty cycle” description applies to the movement of the actuator. However, “duty cycle” is not an accurate comparison because the flow rate in the channel takes much longer to decay than the 7 second period during which the pump is turned off. This is discussed more later. Another consideration is that the stage mounted to the actuator is spring-loaded and adds complication to the analysis. This spring action actually allows the plunger to be pushed at a rate slower than the $0.5 \mu\text{m/s}$ that the actuator is moving.

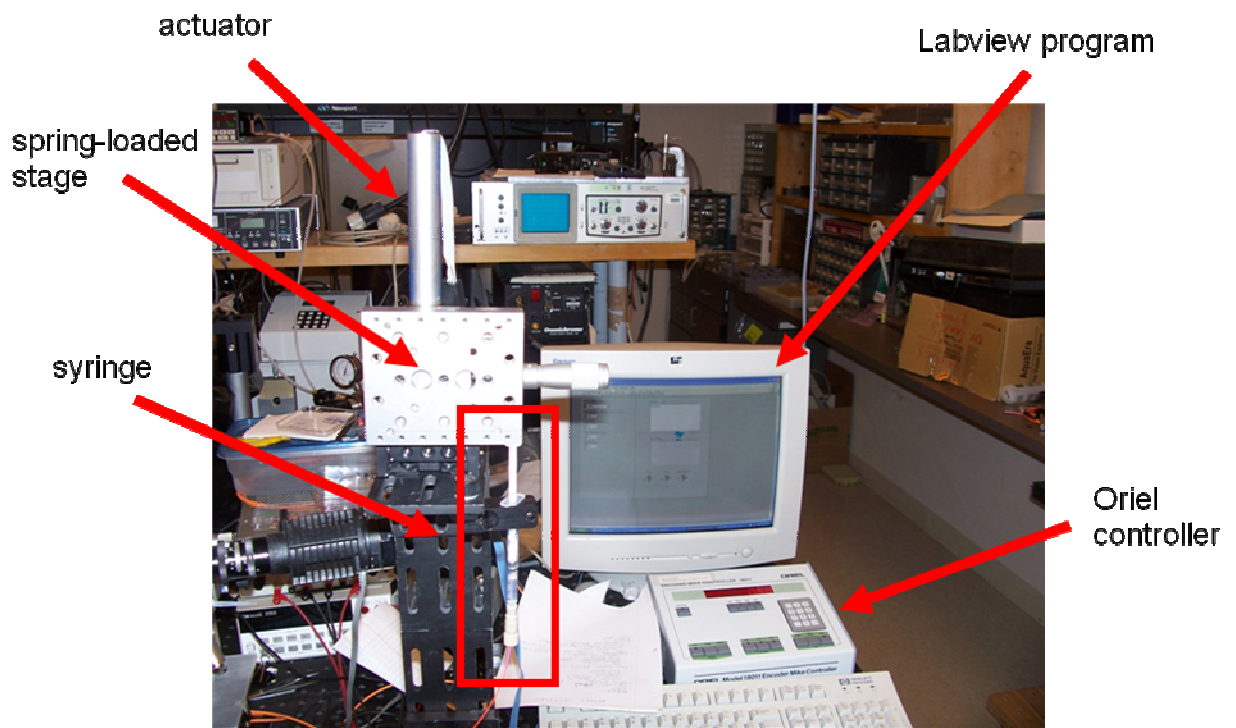


Figure 4

Through experimentation, it was quickly discovered that the derived equation does not hold true for glass chips, but is reasonable for PDMS chips. This is because the actual cross-section in a glass chip's channel is larger and cannot be accurately estimated. Experimentation also revealed that due to complex pressure dynamics, the flow rate in the channel does not follow the syringe plunger. To be more precise, when the plunger is moved and then stopped, the flow in the channel does not stop immediately, but rather decays over the course of several minutes. This behavior is analogous to the behavior of an RC circuit. Both have a time constant associated with how long it takes the flow rate to die down. The larger syringe (8.585 mm

diameter) builds up a higher pressure and the time constant is several times longer than the time constant for the smaller syringe (4.699 mm diameter). This suggests that the cross-sectional area of the syringe is proportional to the time constant for the flow rate inside the channel. All of these more complex dynamics make experimentation the best indication of actual flow inside the channel. There was no precise way to obtain the velocity of spheres moving in the channel but the duty cycle described earlier is estimated to produce a flow rate of 40 $\mu\text{m/s}$ in a PDMS channel. Due to limited fabrication of glass chips near the end of the semester, the duty cycle for the desired flow rate in a glass chip has not been found. However, it is known that the duty cycle must be higher than that for the PDMS channel.

Second Semester Updates

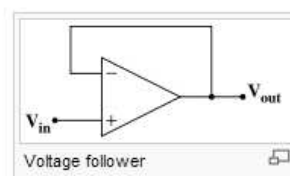
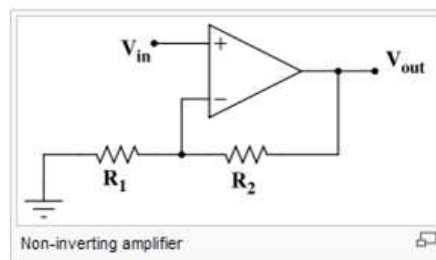
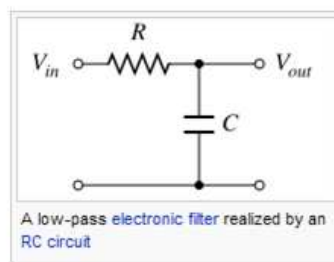
Spheres often get trapped on the edges of the drilled hole when pumping a solution through the channel. To deal with this problem, a new set of solutions were made and documented. These solutions are more dilute and should allow for operation with less clogging. The new 9.77 μm sphere solution is 0.05 cc of sphere solution to 7 cc of de-ionized water. The new 7 μm sphere solution is 4 cc of sphere solution to 10 cc of de-ionized water.

Perhaps the most prominent problem that hindered the project is leaking chips. Chips often leak at the nanopore-glass barrier. Another common place that chips leak is the edges of the chips where the glass-to-glass bonding or PDMS-to-glass bonding occurs. Glass-to-glass bonding problems cause leaking and this problem is more extensively discussed in Chapter II: Channel Fabrication. Many leaks cause fluid to flow outside the channel or not in the channel at all. The most effective method of fixing leaking chips is UV glue. However, UV glue can only be used to patch the outside of a chip, not where glass-to-glass or PDMS-to-glass bonding has failed. Therefore, patching the perimeter of a chip or the nanopores can prevent leaking, but not flow outside the channel within the chip. The UV glue is mostly transparent and does not harden until exposed to ultraviolet light. After applying UV glue to the necessary part(s) of the chip, the glue must cure in the ultraviolet light for at least 5 minutes. Experimentation has found that 15 minutes of curing seems to be more appropriate.

Chapter V: Detection Circuit

We needed to be able to tell when a cell was present in our system. For this we decided to design a detection circuit. This circuit would detect a cell by a modification in the light intensity. In order to design the detection circuit we started with a ST connectorized photodetector (OPF482) connected to a 62.5 μm core diameter multimode fiber optic cable. The light from an infrared LED goes into the microscope and then through the fiber optical cable into the photodetector. A photodetector is a photodiode which is a component with a p-n junction.

When a photon, light, of sufficient energy strikes the diode, it excites an electron in the valence band thereby creating a mobile electron and a positively charged electron hole. If the absorption occurs in the junction's depletion region, or on average one diffusion length away from it, these carriers are swept from the junction by the built-in field of the depletion region, producing a photocurrent. Photodiodes can be used in either the zero bias mode, known as the photovoltaic mode, or in the reverse bias mode, known as the photoconductive mode, the mode we are interested in. In the zero bias mode, light striking the diode causes a current across the device which leads to a forward bias of the diode which in turn induces “dark current” in the opposite direction to the photocurrent. Dark current is the relatively small electric current that flows through a photodiode even when no photons are entering the device. This is called the photovoltaic effect and is the basis for how solar cells work, which are just a large number of big photodiodes. Onto reverse bias which only induces a little current (known as saturation or back current) along its direction. But a more important effect of reverse bias is widening of the depletion layer (therefore expanding the collection volume) and strengthening the photocurrent. Circuits based on this effect are more sensitive to light than ones based on the photovoltaic effect and also tend to have lower capacitance due to the greater separation of the charges, which improves the speed of their time response, because $\tau = RC$ so the smaller the capacitance the smaller the time constant. On the other hand, the photovoltaic mode tends to exhibit less electronic noise. Another type of photodiodes is the avalanche photodiodes which have a similar structure, but are operated with a much higher reverse bias which allows each photo generated carrier to be multiplied by avalanche breakdown resulting in internal gain within the photodiode, which increases the effective responsivity of the device. Our photodetector is used in reverse bias with a large resistor (1.8M Ω) to have the majority of the



current flow into the circuit. The next step of the circuit is a low-pass filter with a cutoff frequency of 1,000 Hz to reduce the noise from the photodetector. The output from the filter goes into the operational amplifier or op-amp. The op-amp, a LF412CN, is setup in a non-inverting configuration with a gain $(1 + R_2/R_1)$ of 2,500. After the op-amp stage, we have a voltage buffer or voltage follower, used as a buffer amplifier, which is used to eliminate loading effects or to interface impedances. $V_{out} = V_{in}$ with $Z_{in} = \infty$ in theory, but in reality it is the input impedance of the op-amp, which is usually $1M\Omega$ to $1T\Omega$. Some of the difficulties we ran into were a noisy signal, which is why we added a low pass filter, having the op-amp oscillate so we added some capacitors to eliminate this. We also had a weak input signal which is why we increase the resistor to $1.8M\Omega$. Below is the final circuit

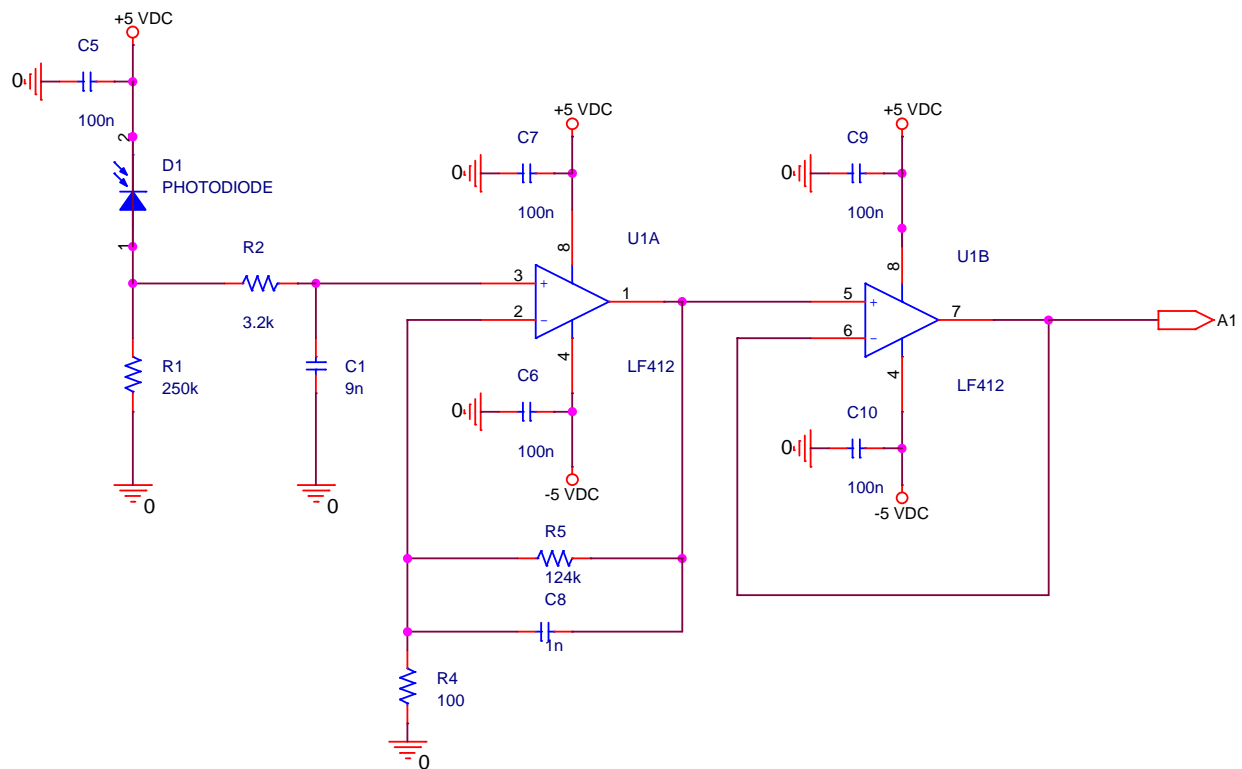


Figure 5.3

Second Semester Updates

Due to many problems with the previous circuit design such as noise causing errors in our results and simply not enough gain, we redesigned the entire light modulation detection circuit.

The redesigned circuit (Figure 5.4) is still based around the premise of the previous circuit's transimpedance stage, but uses a different configuration. It was seemingly problematic to use a resistor based transimpedance such as R1 in Figure 5.3 to generate a voltage based off of the photocurrents, as the photocurrents ranged from 900 nA to 5 μ A and the amount of external electromagnetic interference seemed to be enough to cause erroneous values. The redesigned circuit takes advantage of a transimpedance amplifier (TIA) configuration shown in figure 5.4 as well as a voltage amplifier.

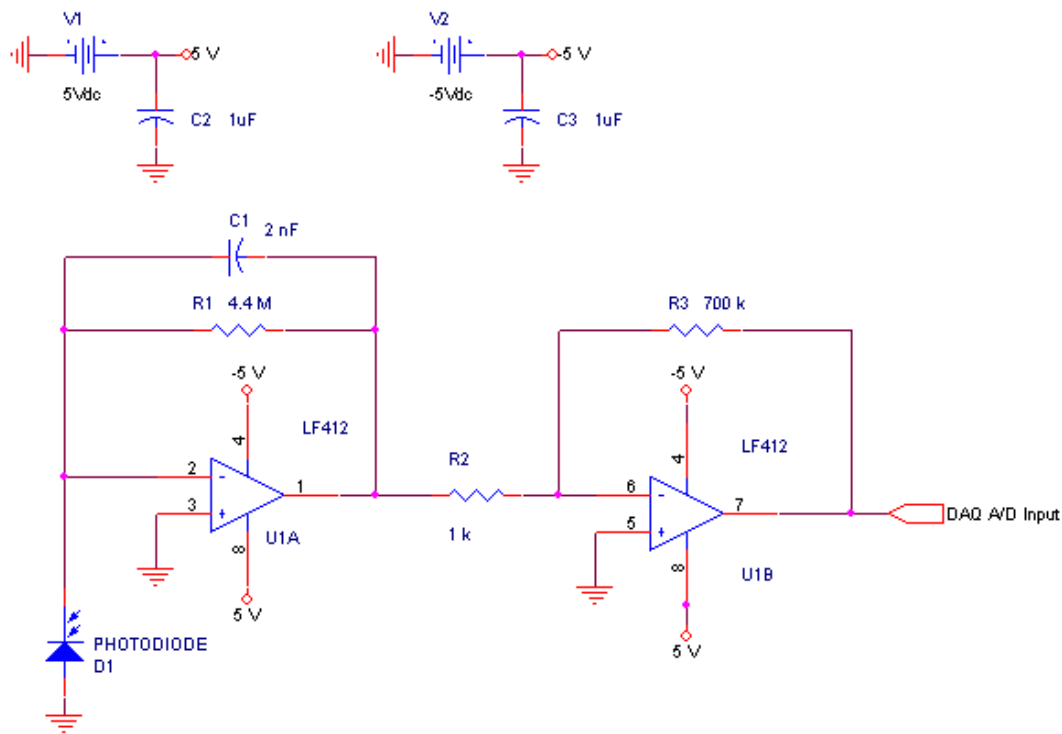


Figure 5.4

The first stage of the circuit (Figure 5.5) is the TIA with a transimpedance gain of $4.4\text{M}\Omega$. The second stage of the circuit (Figure 5.6) is the voltage amplifier, taking the voltage output from the TIA and applying a gain of 700 V/V .

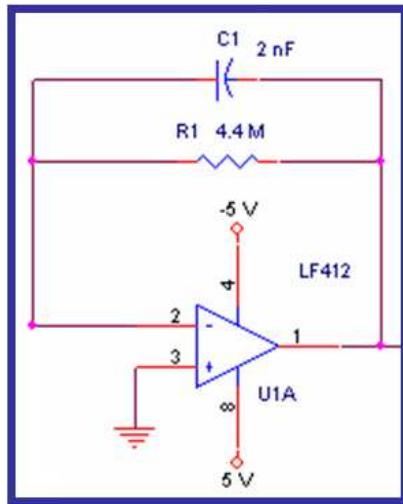


Figure 5.5

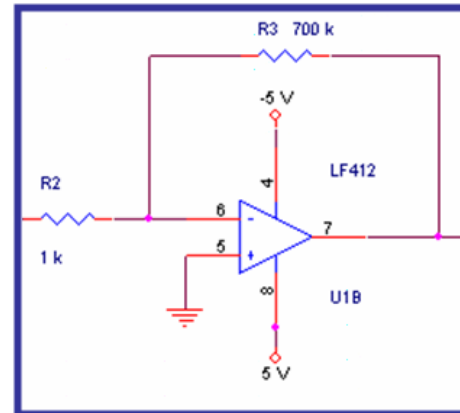


Figure 5.6

Noise was still seen as a problem with this new circuit. Noise of about 60 Hz was seen on the output of our amplification stages, which caused unreliable results while automating as it created a $30\text{-}50\text{ mV}$ difference on the output of the circuit. The noise was dealt with by the use of the low pass filter (LPF – Figure 5.7) as well as decoupling the power supplies from the circuit (Figure 5.8). The LPF can be seen as the capacitor C1 in parallel with the feedback resistor R1. This LPF limits the overall bandwidth of the circuit causing a slower time response, but is required to limit the amount of noise from the input signal. The capacitors on the power supplies act to decouple the supply lines from the circuit, which greatly limits the destabilizing effects of the inductive response the supplies cause when applying a load. We also created an aluminum enclosure to house the circuit in order to stop any electromagnetic interference.

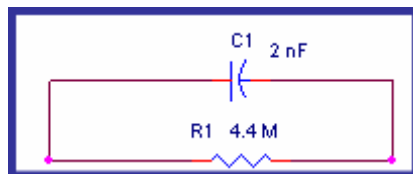


Figure 5.7

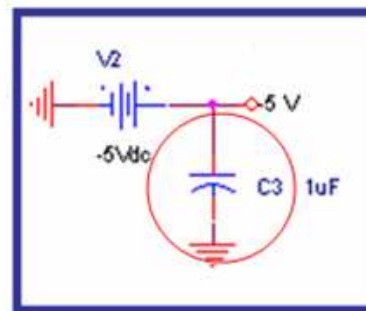


Figure 5.8

The time response is now the biggest issue with the circuitry. The limited bandwidth due to the LPF has caused the overall system performance to decrease. The amplification stage produces the largest time constant of the system, and is the cause of the issues with a slow time response. In order to achieve a faster time response, we could either tweak the LPF for optimal values, or use an op-amp made for transimpedance configurations, such as Texas Instrument's OPA380. What this amplifier provides over our current op-amp, the LF412, is a much larger gain bandwidth allowing for a greater input signal bandwidth, and also offers great precision and low noise which is important when trying to amplify currents as low as 1 nano-Ampere.^[5]

A future design idea, which would call for a complete redesign of the circuit, would include an op-amp like the OPA380 and a voltage buffer. To achieve the best distortion reduction and performance in a transimpedance circuit, all required gain should be taken care of with the TIA.^[4] The output of the gain stage should be followed by a voltage buffer. The same noise cancellation ideology and capacitive decoupling should be followed from previous designs; however the low pass filter should be tweaked to acquire a stable phase margin. Ideas for improving performance with a transimpedance circuit can be found in the datasheet for the OPA380^[5].

Chapter VI: RF Switching

To fully automate the system, the cell traps would have to be turned on when a cell is in proximity of a trap. To do so, the Data Acquisition Unit (DAQ) would monitor the voltages from the cell detection circuit until the given voltage exceeds the threshold, showing the presence of a cell. The DAQ would then create a digital high output on an analog switch or relay and cause a signal of radio frequency (RF) to be applied to the traps, thus causing a cell to be trapped in an electromagnetic field. The components we tried to use to switch the RF signal, such as an analog switch, no longer performed as an ideal switch due to the high frequencies. At RF, the capacitance associated with the analog switch caused a percentage, usually 10%, of the signal to leak when the switch was considered open. To avoid problems with RF signals, we chose to use a Teledyne 172-5 RF DPDT relay, which is designed to handle RF signals.

Chapter VII: Dielectrophoretic (DEP) Trapping

DEP trapping is necessary in this project for one main reason: If the sphere/cell/particle is not held in a particular position without moving, a spectral reading of light shined through that object will be extremely difficult to gather data with the equipment and limited budget that we have. DEP trapping is a method of using electromagnetic forces to hold an object in place. One might ask the question: how do you exert a force upon a charge neutral object using an electric field? The answer to this question is not trivial. DEP trapping occurs when a non-uniform electric field is passed through a neutral body. Internal to the neutral object, the molecules within the neutral object polarize, much like the depletion region that occurs when a voltage is put across a pn junction. The imbalance of localized charges results in a virtual electric dipole being formed within this neutral object. Therefore, the electric field will “apply” a force to the surface dipoles in the overall neutrally charged object. Since the objects we are concerned with are on the order of 10 μm in diameter, it is easier to exert a significant enough force on these small particles with large surface to volume ratios to “push” them into a suitable area to take a spectral reading.

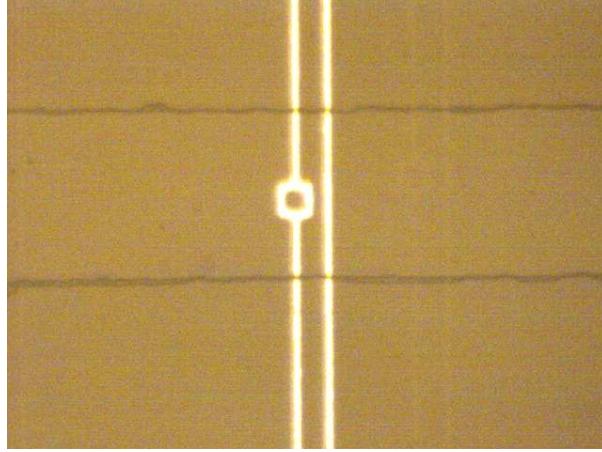


Figure 6.1 Picture of DEP trap electrodes

In order to achieve a non-uniform electric field, a time-varying voltage must be applied across the electrodes of the DEP trap. The approximate force applied to an object being trapped can be defined by the formula

$$\mathbf{F} = 2\pi\epsilon_1 R^3 \text{Re}[\underline{CM}(\omega) \times \nabla \underline{E}^2(\mathbf{r})] \quad [1]$$

where F refers to the dipole approximation to the DEP force, ϵ_1 refers to the permittivity of the medium surrounding the object being trapped, R is the radius of the particle, r is the spatial coordinate, ω is the angular frequency of the applied voltage, E is the complex applied electric field, CM is the Claussius-Mossotti factor. The Claussius-Mossotti factor is a frequency dependent function of the permittivity of the medium outside the particle and the inside of the particle. In simpler terms, the force to push an object into a trap is proportional to the positional gradient of the electric field. The implications of such a thing is that the particle will experience a force until it reaches an extrema in the intensity of the electric field (i.e. the positional derivative of the electric field is zero, and therefore the force will equal zero.) This translates into basically a restoring force that keeps the particle trapped at a certain point until the electric field is removed or until a much larger force physically removes the particle from the trapping area.

In the scope of this project, the non-uniform electric field comes from a 5 Vpp sinusoidal signal across the two electrodes of the traps.

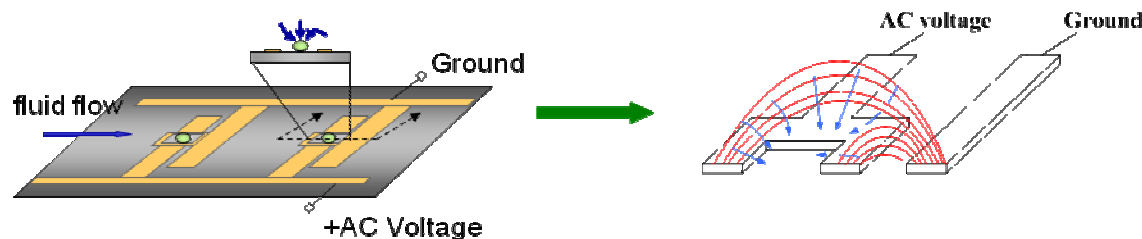


Figure 6.2 (a): Electromagnetic Modeling of DEP traps. Reproduced from [2].

Based upon the field lines shown in Figure 6.2, the point of highest electric field intensity is approximately in the center of the trap. This provides an optimal trapping point for which the spectrometer can take a reading.

Chapter VIII: Future Work

Chip bonding has shown to be a critical step in chip fabrication. Failures in PDMS and thermocompression bonding have not been reliable methods for bonding the trap and channel pieces together, and more reliable methods need to be found.

With so much variance in chip fabrication, it would be beneficial to create a feedback control system for flow control. While the current flow control method can achieve desired flow rates, the velocity of particles in the channel and the volume of throughput are currently human estimates. Different chips sometimes require different settings in Labview to achieve the same result. If an accurate way to measure flow rate were achieved, a feedback control system could allow for the same flow rate even if there are variances in the effective cross-sectional area of chips' channels.

The optical system will need to be fine tuned to allow for adequate light modulation on chips with dielectric coating. This coating significantly reduces the transmitted light intensity (transmitted power). If we are able to obtain any donations, a higher output infrared LED could improve the system. Also, if a high performance photo diode was obtained the performance may improve. Last, the optical detection circuit could be improved in the area of time response. Using a high-performance transimpedance amplifier designed for photocurrent amplification may enhance performance. This amplifier should have a larger gain-bandwidth product to allow for higher frequency response while maintaining the necessary gain and signal-to-noise ratio.

In the future of the project, the spectrometer will become an essential part of the cell analysis. Data acquisition will need to be automated using Labview software and resulting data of the cells will allow for cell differentiation. Because it is the shifting of the wavelength that

differentiates cell types, the spectrometer is the heart of the system. Triggering DEP traps based on light modulation (i.e. intensity) is very difficult and may not be feasible with current project limitations. An alternative to trapping based on light intensity would be to use the spectrometer and attempt to detect changes in wavelength and trigger the DEP traps accordingly. It may even be possible in the future to skip the trapping step entirely and simply take data of the cells' spectrums as they pass. Such alternatives should be investigated along with other possibilities to improve the rate at which cells can be analyzed.

Another key element to automation is software. Once the spectrometer is implemented and spectral data is taken, the data needs to be stored in an efficient filing system and analyzed for the end user. Without software, each spectrum would have to be analyzed by a person and compared to other data. The software should have statistical data about the analyzed cells and should have tolerance parameters that can be set by the user to specify what characteristics determine different cell types.

REFERENCES

"What is Optofluidics?" Optofluidics. 2007. 10 Dec. 2007

<http://www.optofluidics.caltech.edu/optofluidics/index.html>

Yang, Changhuei, and Demetri Psaltis. "Optofluidics: Optofluidics Can Create Small, Cheap Biophotonic Devices." Laser World. 1 July 2006. 10 Dec. 2007

http://www.laserfocusworld.com/articles/article_display.html?id=259933

[1] J. Voldman, R. Braff, M. Toner, M. Gray, and M. Schmidt, "Holding Forces of Single-Particle Dielectrophoretic Traps," *Biophysical Journal*, Vol. 80, pp 531-541, January 2001.

[2] W. Wang, H. Shao, K. Lear, "Lab-on-a-Chip Single Particle

Dielectrophoretic (DEP) Traps" powerpoint presentation given March 2006.

[³] Lear, Kevin L., Hua Shao, Weina Wang, and Susan E. Lana. "Optofluidic Intracavity Spectroscopy of Canine Lymphoma and Lymphocytes." IEEE Explore 4 Dec. 2007.

[4] McGoldrick, Paul, ed. "TI OPA380." Wireless ZONE. 10 May 2004. 20 Mar. 2008

http://www.en-genius.net/site/zones/wirelessZONE/product_reviews/hfp_051004

[5] "OPA 380." Texas Instruments. Sept. 2007. 20 Feb. 2008

<<http://focus.ti.com/lit/ds/symlink/opa380.pdf>>.

APPENDIX OR APPENDICES

- Appendix A: Abbreviations

AC – Alternating Current

DAQ – Data Acquisition Unit

DC – Direct Current

DEP – Dielectrophoretic

LED – Light Emitting Diode

OFIS – Optofluidic Intracavity Spectroscopy

OpAmp – Operational Amplifier

PDMS – Polydimethylsiloxane

VI – Labview Virtual Instrument

V_{pp} – Volts Peak-to-Peak

- Appendix B: Budget

- ADG 452 Digital Switch -- \$15
- Various circuit elements including Op-amps and digital chips -- \$10
- Hytek iUSBDAQ U120816 -- \$105
- TOTAL EXPENSES = \$130

Starting Budget = \$500 over 2 semesters

Money left = \$500-\$130=\$370

- Appendix C: Peripherals

The need for peripherals in this project is abundantly apparent. We used many different measurement and control systems to be able to achieve our goals. These peripherals were:

- Data Acquisition Unit (iUSBDAQ-U120816) from Hytek Automation
- Ocean Optics Spectrometer (HR2000)
- Oriel Instruments Encoder Mike Controller (18011)
- Microscope (heavily customized Olympus 230997)
- Logitech USB camera
- Beam splitter (Newport parts manufactured in-house)

C1: Data Acquisition Unit

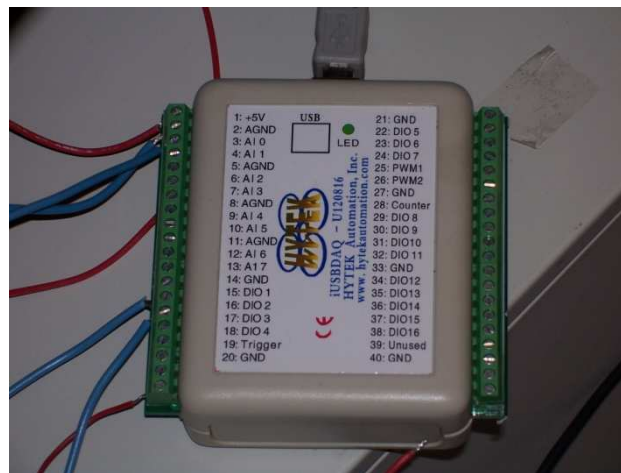


Figure C1.1 Hytek Data Acquisition Unit

The data acquisition unit was brought on board due to a need for triggering a circuit based on amount of light collected by the photodiode. This made it so that instead of creating a new logic circuit every time we changed the gain stage of the amplifier, the logic could be controlled with a Labview VI. This also took out the guess work for a logic chip. In the specification sheet for a 7400 series logic component, there was a large range of voltages that were specified to be undefined logic. The DAQ took a lot of the uncertainty out of the logic. The DAQ is accurate to within 3 mV DC on its 8 available channels of analog inputs. It also can

output digital logic at 5 V DC on one of its 18 Digital I/O channels. This may seem like it's overkill to have so many, but the DAQ was 2/3 of the price of some of the other data acquisition units that are on the market. It has a sampling rate of 13,000 samples per second on a single channel. More expensive units were about the same or even worse. We designed a Labview VI that would take an analog input, compare it to some specified reference, and output a digital signal based upon whether or not it was higher or lower than the given reference.

Here is the front panel of the Labview VI:

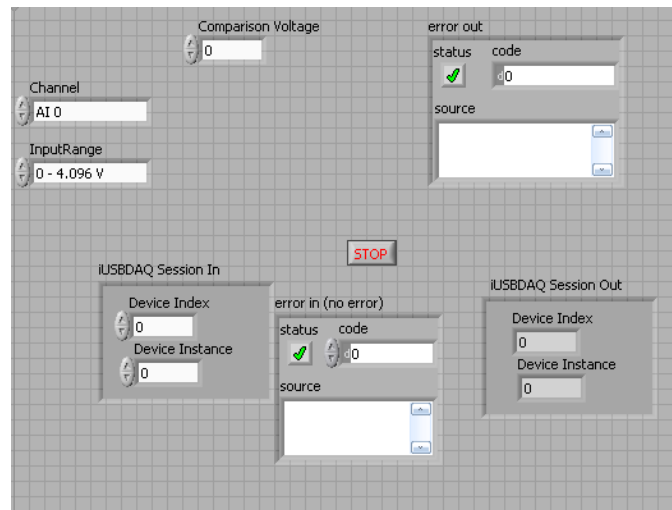
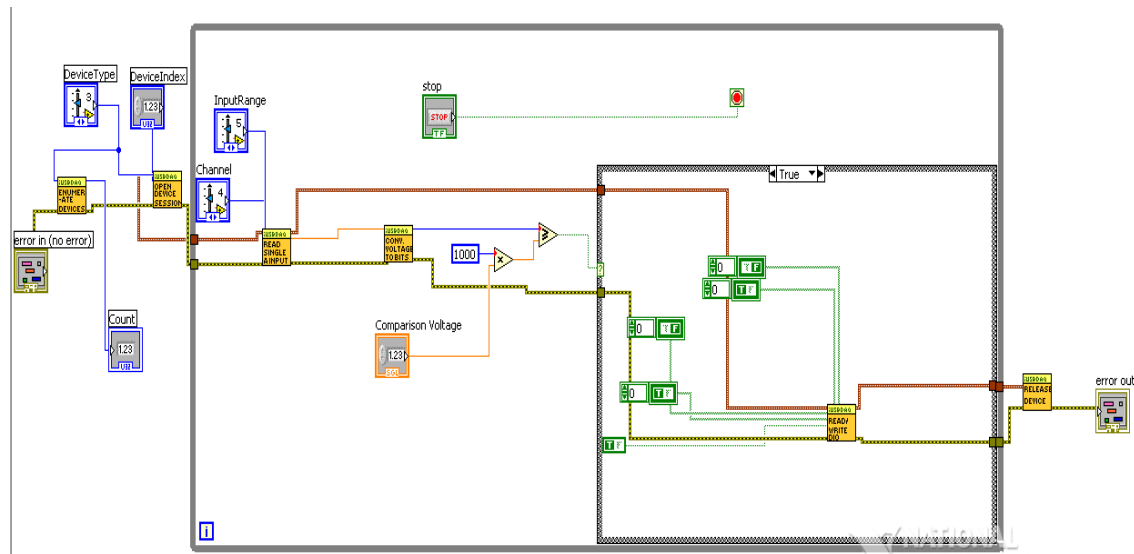


Figure C1.2 Front Panel of DAQ VI

The interface is quite simple. The triggering voltage is input in the field labeled “Comparison Voltage”. The channel of the analog input is easily configured. Any errors are easily read on the error out field. Since we configured the DAQ to take inputs on analog channel 0 (the default value), getting a digital output based upon comparing to a preset voltage was as easy as inputting the comparison voltage, and hitting the run button in Labview.

The VI for controlling the DAQ was not difficult to program. Another reason we went with this DAQ was due to the fact that Labview VI's were available on the Hytek Automation website. This made it so that it was a “plug and chug” type of program.

Here is the VI block diagram:



Figure

C1.3 Block Diagram of DAQ VI

The algorithm used for trapping is described as follows:

Stage 1: The first thing that needed to be done was to be able to read the output of our light modulation circuit. This was accomplished by using the Hytek Data Acquisition Unit. The Hytek has analog to digital capabilities, and drivers available on the Hytek website to allow for a conversion of an analog signal to a 16 bit floating point number. This allows for approximately three decimal place precision on the readings from the light modulation circuit.

Stage 2: Once the reading is taken from the light modulation circuit and converted to a floating point number, the second thing that is done in this algorithm is to compare that number to a fixed value. The fixed value that we have been using is the average voltage reading from the light modulation circuit when no sphere is present within the trapping area and the reading when there is a sphere present. This creates a buffer by which particulates and various fluctuations in the output voltage would not set off the traps. For example, generally the output voltage without a sphere in the trapping area is approximately 3 V. When a sphere is in the trapping area, the voltage drops to 2 V. Therefore the comparison voltage would be 2.5 V. That way, if a small particulate were to flow into the trap area, we would not have a false trapping. Also, if the voltage of the output were to fluctuate by 10% without a sphere being in the trap, the worst case scenario would be a 2.7V output vs. 3V. This would still allow operation to work without creating a false trapping situation.

Stage 3: Once the comparison occurs, it sets the value of a boolean variable. This boolean is true if the voltage was less than the fixed value and false if greater than the fixed value. If a false is generated in this boolean variable, then the algorithm goes back to stage 1 to read in a new value. If a true is generated, then the Hytek's capabilities are exploited again. The Hytek has drivers to

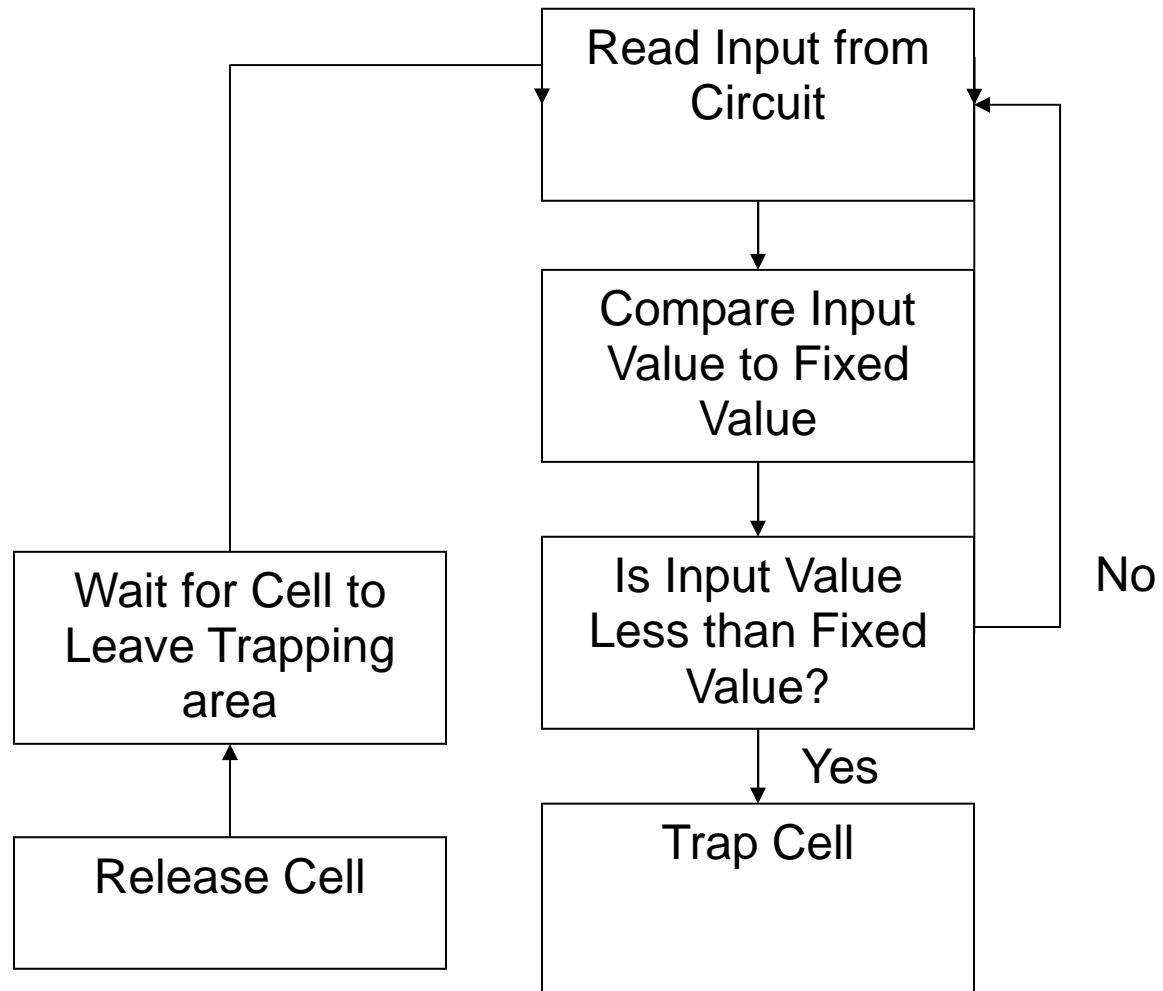
send out digital signals of either 0 or 5V. When the boolean variable is true, the Hytek sends a digital signal to apply an RF signal to the traps, theoretically trapping the cell.

Stage 4 (future work): Once the cell is trapped, the spectrometer will take it's reading, store it in a file to be read by the user. This has not yet been implemented, but it is planned to be done in the future. Currently, we are modeling this as a delay of 500 ms.

Stage 5: Once the spectral reading is taken, the digital signal that is applied to send the RF signal to the traps is set to 0V, and the sphere will be released.

Stage 6: In order for there to be no “re-trapping” of the same cell, there is a small delay of 500 ms after the trap is released to allow time for the recently trapped cell to clear the trapping area before another voltage reading is taken. From this stage, process starts over again until terminated by the user.

Here is a flow chart of the algorithm:



C2: Oriel Instruments Encoder Mike Controller 18011



Figure C.2.1(a) Control Panel of Oriel Controller (b) Microscope stage being controlled

The Oriel Instruments Encoder Mike Controller is normally used as a microscope stage controller to move a microscope stage very slowly. Our application of this piece of equipment was as a syringe pump. The main reason that this was used is because it was able to move a syringe plunger slow enough to get reasonably slow flow within the channel of the chip. The minimum rate at which the actuator can move is $0.5 \mu\text{m/s}$. Remember that the chip only had a cross-sectional area of approximately $5000 \mu\text{m}^2$. The syringe that we are using is approximately 0.5 cm in diameter. This makes it so that the stage must be moving extremely slow in order to get a flow rate within the channel to be as slow $40 \mu\text{m}$ per second, which is the flow rate by which it is suitable to trap cells. Again, we used Labview to control the actuator. This was much more difficult to control because there were no VIs available on the internet. This made for a much bigger challenge because we were unfamiliar with RS-232 communication that was required for control of the Oriel actuator. Using a wiring diagram that was in the User's manual of the Oriel actuator, we created our own RS-232 to DB9 cable to interface between the control panel and a computer.

Block Diagram

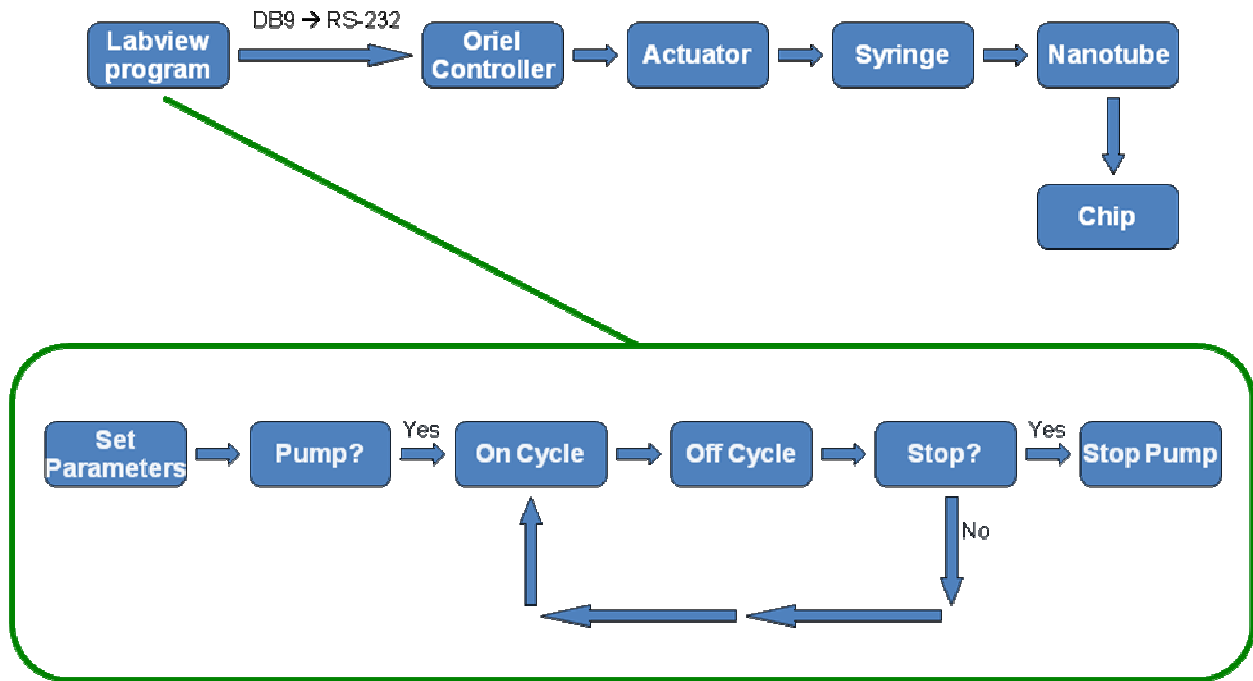


Figure C2.2



(a)

(b)

Figure C2.3(a) RS232 input to Oriel Controller

Figure C2.3(b) DB9 input to computer

A Labview VI controls the signals that are put on the different wires of the RS-232 Cable. The front panel for the Labview VI looks like this:

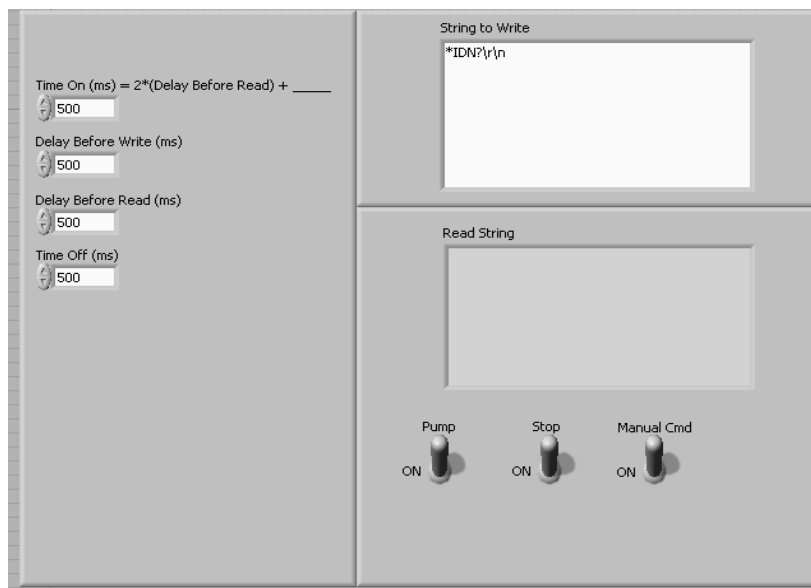


Figure C2.4 Front Panel of Oriel Controller VI

The switches in the lower right portion of the front panel control what the switch actually does. Only one switch can be on at one given time in order to function properly. When the VI is run with only the pump switch on, the pump will run for a total of $2 * (\text{Delay Before Read}) +$ the time value(ms) specified in the top left input box. When the VI is run with the stop switch turned on, it will stop all pumping functions. With only the manual command switch turned on, a string will be sent to the Oriel controller. For example, the string “V200/n” will command the Oriel actuator to move at a velocity of 200 $\mu\text{m}/\text{second}$. There are many commands like this that the VI already uses to control the actuator within the VI itself, such as run and stop. The way that the pump command works is that it will send a run command. Then there will be a specified delay time, followed by the stop command being sent to the controller, then a second specified delay. The loop starts over starting with a run command. This allows the user to specify a duty cycle for the pump. The values that we used for this VI were: time on = 725 ms, delay before write = 50 ms, delay before read = 50 ms, and time off = 7000 ms. This roughly gave a flow rate of 40 μm per second. The VI block diagram shows all of the internal logic that occurs with the switches, and with the delays, as well as the Run and Stop commands sent to the Oriel actuator.

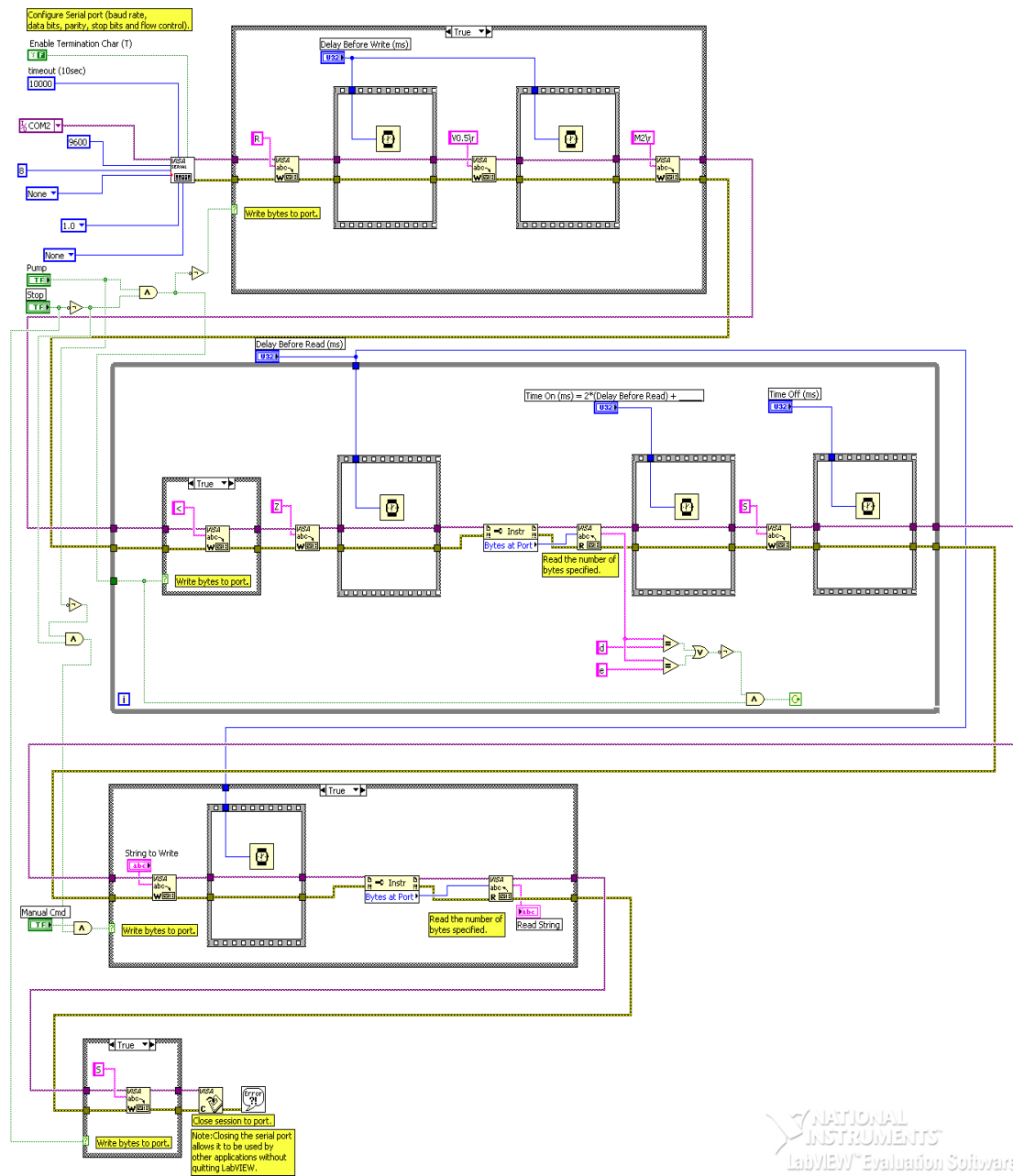


Figure C2.5

NATIONAL
 INSTRUMENTS
 LabVIEW™ Evaluation Software

C3: Ocean Optics HR2000 High-Resolution Fiber Optic Spectrometer



The overall goal of the project is to differentiate cells as they pass through the channel. In order to do this, the method of intracavity spectroscopy will be used. In order to detect the changes in wavelength as a cell passes through, a spectrometer is used to analyze the diffraction of the LED light source. At this point in the project, the spectrometer has only been used to assist with the setup of the optical system. The spectrometer was used to maximize the light intensity from the LED light source as well as the focused LED light after it has passed through the lens. The resulting spectrum also provided verification that the microscope optics were properly aligned. Narrow peaks in the spectrum indicated proper alignment from the LED light source to the microscope.

- Appendix D: Project Tips and Tricks

D1: Attaching Nanoports

The recommended procedure is below:

1. Clean the chip around the drilled hole and the bottom of the nanoport using acetone, methanol, and de-ionized water. It must be cleaned in this order using 3 different Q-tips to scrub the surface. The next “cleaner” must be applied before the previous one dries. Putting the specimen to be cleaned in a glass dish is usually easier in that there can be an excess of the cleaner, making it take longer to dry. It must be glass because plastic reacts with acetone. Use an air gun to blow the surface dry before the de-ionized water dries. Remember to wear gloves when working with acetone and methanol.
2. Flip both the chip and the nanoport upside down so that the surface of the chip that will be bonded is facing downward and the surface of the nanoport that will be bonded is facing upward.
3. Center the o ring on the nanoport surface and bring the nanoport into contact with the chip, centering the nanoport over the drilled hole on the chip. Notice that the o ring should be between the chip and nanoport.
4. While holding the nanoport in place, use a pair of tweezers to grab the sides of the nanoport and press it against the chip while applying pressure on the *center* of the opposite side of the chip with a finger. This should allow the placement of a clamp over the nanoport and chip, holding the 2 together, without fingers in the way.
5. Place a clamp over the nanoport and chip holding the 2 together. Make sure that the clamp is centered and applying even pressure across the nanoport surface before releasing the tweezers hold on the nanoport.
6. Put the chip with the nanoport clamped on in the oven and bake it at 170°C for 1 hour.
7. Remove the chip from the oven and allow to cool.

D2: Optical Calibration

At the heart of the OFIS process is the microscope. This is the instrument that we use to gather light to use for spectroscopy, cell detection, and for the camera. No other instrument needs to be calibrated as frequently as the microscope, and no other instrument in the process can dramatically change the resulting data by a slight adjustment. Therefore the correct calibration of both the microscope and the light source is vital for any reasonable data collection from a microfluidic sample. In this section, the calibration process of the microscope will be covered. The difficulties in learning how to calibrate the microscope will also be explored.

To begin, the basic knowledge of how our system works is essential. Below, is a figure on the general set up of the entire system. The size of the optic fiber coupled into the beam splitter should be around 50/125 to 62.5/125, and needs to be a multimode fiber. The percentage of light sent through the optic fiber is 90%, while the remaining 10% of light goes to a camera. In the system, an infrared LED is used as a light source. Using a lens, this light is focused to a small spot on the microfluidic sample where chips are placed to provide high light intensity. The light that goes into the microscope is then split as described above. Optical fibers then transport the light to the spectrometer and cell detection circuit (not pictured).

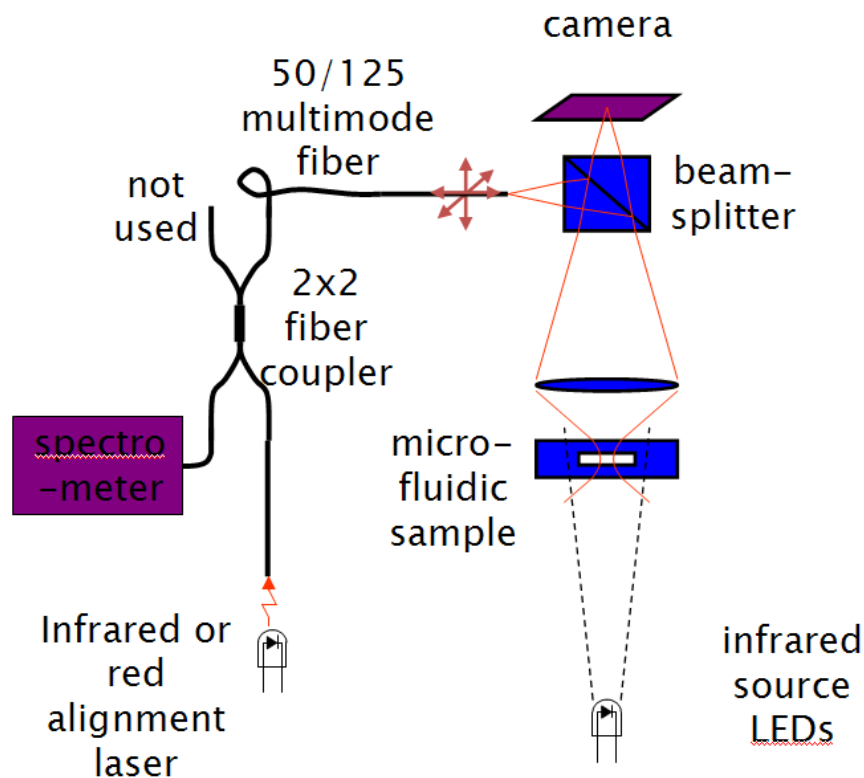


Figure D2.1: Diagram of microscope being coupled with light source

Calibrating the optical system is a fairly involved process with many steps and can take several hours. To calibrate the optical system, follow the steps below:

1. This first step is not truly necessary, but serves as a good reference and is a good way to start. To get a starting point for calibrating the system, the use of a LED that emits light in the visible spectrum is useful. Setup the visible-light LED below the microscope stage and drive the LED to emit light. Place a white piece of paper on the focusing plane (the microscope stage, where chips will be placed) and use the focusing lens for the LED to focus the visible light on the same plane (the piece of paper). The goal of the lens above the LED is to make the light emitted from the LED confined to a very small area in a circular shape. Note that the lens should be fairly level if the LED, lens, and focal point are aligned vertically. Once complete, remove the piece of paper.
2. Turn the microscope light on. Center the infrared LED below the lens where the microscope light falls (after passing through the hole in the stage and the lens) and connect it to a current source for operation. Now turn off the microscope light.
3. Carefully rotate the lens out of the path between the LED and microscope (without changing its height or tilt).
4. Turn on the spectrometer and set it up to take intensity counts. Note that you must ensure that the optical fiber is connected between the microscope and spectrometer. Set the reference level for the spectrometer with no light source.
5. Turn on the infrared LED with a 50 mA current. Adjust x and y tilt of the LED to maximize the intensity counts that the spectrometer reads.
6. Now reposition the lens over the LED (and under the stage). Fine tune (adjust) the position, tilt, and even height of the lens to maximize the intensity counts on the spectrometer. We achieved counts of around 3000. Note that although the height should not have to be repositioned after step 1, fine adjustments often improve the intensity.
7. Turn off the spectrometer and place a chip on the microscope stage. Use the camera to focus the microscope on the center of the chip's channel using the infrared LED as the light source.
8. Once focused, turn the infrared LED off. Connect an alignment laser (preferably in the infrared region) to transmit into the viewing plane through an optic fiber. This is

basically shinning light in the opposite direction back onto the chip (like from the spectrometer back to the beam splitter and then the microscope).

9. Light from the laser is seen in the viewing plane via the camera. Adjust the beam splitter until the laser light is confined to a small, circular area. Our best calibration had a focal point that was on the order of 10 μm to 15 μm in diameter. This ensures that the output from the beam splitter is collecting light from an area where the LED light is focused on and that a cell in this focal point will produce significant light modulation. It is important while doing this that the laser is at a low power output so that the camera is not saturated. With our infrared laser we used 0.2 to 0.3 mA of current to drive output.



Figure E2.2: Example of alignment using a laser

10. Mark the spot on the computer monitor with a marker. Do not move the camera window on the computer after this mark is made. Turn off the laser and connect the optical fibers for normal operation with the detection circuit.
11. Turn on the power supplies for the detection circuit. With the chip still in place, turn on the infrared LED source. Using the marked spot on the computer monitor, verify that in the open channel there are a few volts output from the detection circuit. Also, by positioning the marked spot over DEP trap leads and/or other objects in the channel, verify that the minimum voltage outputs are obtained when the spot is directly over these objects. Optical calibration is now complete.

The difficulties encountered in the calibration of the microscope were numerous, and were mainly due to the poor maintenance of the entire instrument. The second difficulty is the basic concept of the optics.

The microscope used for our experiments has been poorly maintained. Dirt and scratches on the lens are present, which may alter the light collection, but to a lesser degree. The beam splitter stage was unstable and poorly fitted onto the microscope, and due to budget constraints has to be fastened to the microscope with zip ties. If our budget constraints allow, we can machine better housing for the beam splitter. The focusing plane where the micro-fluidic channels sit is also difficult to use with the channels. Scotch tape is required to steady the chip in place and leveled with the focusing plane. The use of tape leads to oils from the fingers being deposited onto the chip, which alters the light characteristics of the chip. Again, if our budget would allow, we could machine a better focusing plane that would allow us to secure the chip into place and avoid taping it. The fiber optic output from the beam splitter is also difficult to use at time, as there is no relief at the ST junction for the fiber optic cable. A relief at the ST junction would allow for the focal length from the optic fiber to the beam splitter to be changed without causing stress to the fiber optic cable or having to disassemble the output of the beam splitter.

The knowledge of optics was one of the easier difficulties to overcome with the help of Dr. Lear. Understanding why we needed a 62.5/125 optic fiber as opposed to a much larger optic fiber is an example of the problems he helped us overcome. The reason why a 62.5/125 cable is used to minimize the area in which the light from the beams splitter is collected.

- Appendix E: Data Sheets and User Manuals

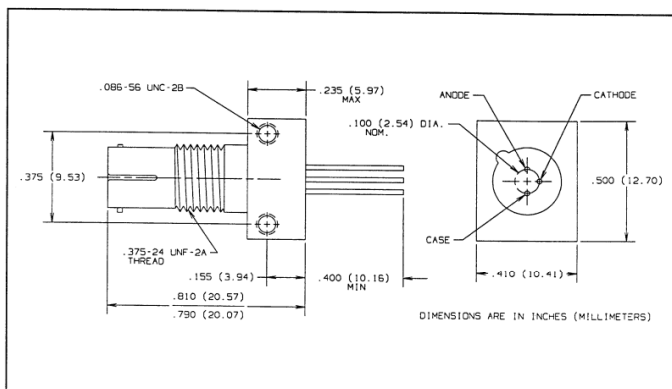
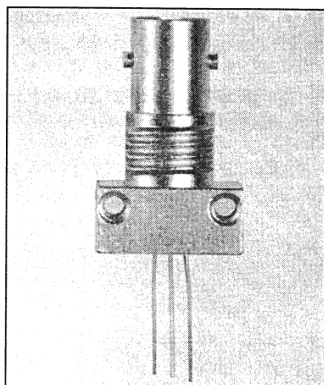
E1: OPF 482 Optic Fiber Photodiode

Product Bulletin OPF482
August 1996



Fiber Optic High Speed PIN Photodiode Type OPF482

in ST* Receptacle



Features

- Component pre-mounted and ready to use
- High speed, low capacitance
- Pre-tested with fiber to assure performance
- Popular ST style receptacle
- Electronically isolated from case

Description

The OPF482 consists of a low cost plastic cap PIN photodiode pre-mounted and aligned in an ST receptacle. This configuration is designed for PC board or panel mounting. Includes lock washer and jam nut, two 2-56 screws, and dust cap.

The PIN Photodiodes are designed to interface with multimode optical fibers from 50/125 to 100/140 microns.

*ST is a registered trademark of AT&T.

Absolute Maximum Ratings ($T_A = 25^\circ\text{C}$ unless otherwise noted)

Reverse Voltage	100 VDC
Continuous Power Dissipation	200 mW ⁽¹⁾
Storage Temperature Range	-55°C to $+100^\circ\text{C}$
Operating Temperature Range	-40°C to $+85^\circ\text{C}$
Lead Soldering Temperature [1/16 inch (1.6 mm) from case for 5 sec. with soldering iron]	240°C ⁽²⁾

Notes:

- (1) Derate linearly @ $2.0\text{ mW}/^\circ\text{C}$ above 25°C .
- (2) RMA flux is recommended. Duration can be extended to 10 sec. max when flow soldering.
- (3) Test @ $V_R = 5\text{ V}$ with 50/125 micron, 0.20 N.A. fiber, @ $10\text{ }\mu\text{W}$ optical power @ 850 nm.

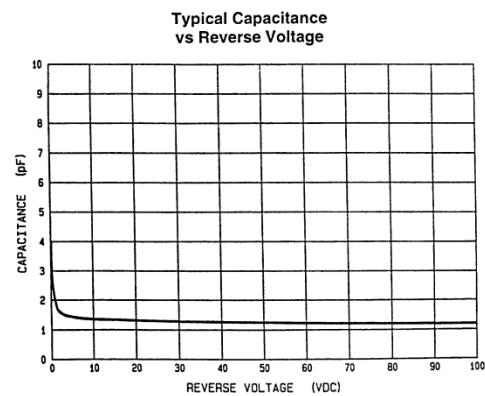
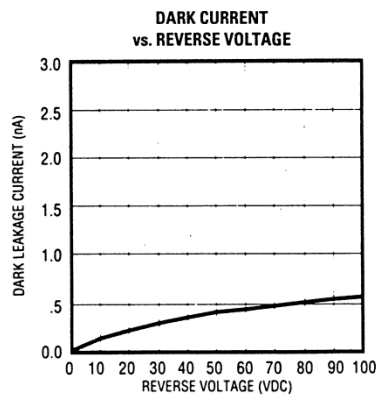
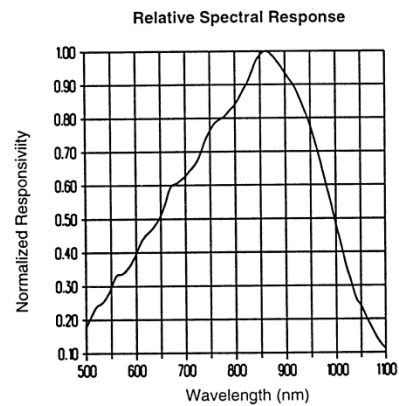
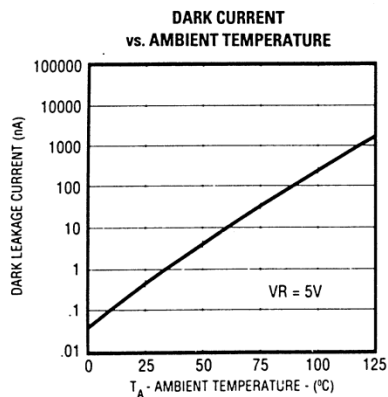
Responsivity levels apply to 50 μm , 62.5 μm and 100 μm core optical fibers.

Type OPF482

Electrical Characteristics ($T_A = 25^\circ\text{C}$ unless otherwise noted)

SYMBOL	PARAMETER	MIN	TYP	MAX	UNITS	TEST CONDITIONS
R	Flux Responsivity	0.45	0.55		A/W	$V_R = 5.0\text{ V}^{(3)}$
I_D	Dark Current		0.1	5.0	nA	$V_R = 5.0\text{ V}$
λ_p	Peak Response Wavelength		860		nm	
t_r	Output Rise Time		0.6		ns	$V_R = 50\text{ V}$, $R_L = 50\ \Omega$, 10%-90%
t_r	Output Rise Time		1.0		ns	$V_R = 15\text{ V}$, $R_L = 50\ \Omega$, 10%-90%
t_r	Output Rise Time		2.0		ns	$V_R = 5.0\text{ V}$, $R_L = 50\ \Omega$, 10%-90%
C_T	Total Capacitance		1.5	2.0	pF	$V_R = 5.0\text{ V}$

Typical Performance Curves



FIBER OPTIC
COMPONENTS

Optek reserves the right to make changes at any time in order to improve design and to supply the best product possible.
Optek Technology, Inc. 1215 W. Crosby Road Carrollton, Texas 75006 (972)323-2200 Fax (972)323-2396

E2: DAQ Comparison

			A/D Characteristics	
	Number of Channels:	Measurement range:	Resolution:	Sampling Rate
DI-148U	8	±10V	10-bit	14400 [Hz]
DI-158	4	Variable - Depends on internal gain setting	12-bit	14400 [Hz]
NI USB-6008	8	±20V	12-bit	10 [kS/s]
LabJack U3	16	±2.4(?)	12-bit	2.5-50 [kS/s]
	Digital I/O			
	Channels		Minimum Required Digital I/O?	
DI-148U	6 bi-directional ports		Yes	
DI-158	4 bi-directional ports		Yes	
NI USB-6008	12		Yes	
LabJack U3	20 (Programmable Ports)		Yes	
	Labview	Cost	Site	
DI-148U	Labview 5	\$50	http://www.dataq.com/products/startkit/di148.htm	
DI-158	Labview 5	\$99	http://www.dataq.com/products/startkit/di158.htm	
NI USB-6008	Yes	\$159	http://sine.ni.com/nips/cds/view/p/lang/en/nid/14604	
LabJack U3	Yes	\$99	http://www.labjack.com/labjack_u3.php?prodId=25	

E3: LF412 Operational Amplifier



August 2000

LF412

Low Offset, Low Drift Dual JFET Input Operational Amplifier

General Description

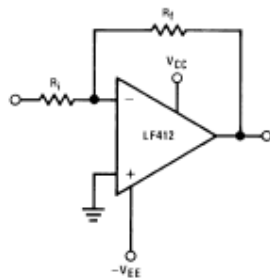
These devices are low cost, high speed, JFET input operational amplifiers with very low input offset voltage and guaranteed input offset voltage drift. They require low supply current yet maintain a large gain bandwidth product and fast slew rate. In addition, well matched high voltage JFET input devices provide very low input bias and offset currents. The LF412 dual is pin compatible with the LM1558, allowing designers to immediately upgrade the overall performance of existing designs.

These amplifiers may be used in applications such as high speed integrators, fast D/A converters, sample and hold circuits and many other circuits requiring low input offset voltage and drift, low input bias current, high input impedance, high slew rate and wide bandwidth.

Features

- Internally trimmed offset voltage: 1 mV (max)
- Input offset voltage drift: 10 $\mu\text{V}/^\circ\text{C}$ (max)
- Low input bias current: 50 pA
- Low input noise current: 0.01 pA/ $\sqrt{\text{Hz}}$
- Wide gain bandwidth: 3 MHz (min)
- High slew rate: 10V/ μs (min)
- Low supply current: 1.8 mA/Amplifier
- High input impedance: $10^{12}\Omega$
- Low total harmonic distortion $\leq 0.02\%$
- Low 1/f noise corner: 50 Hz
- Fast settling time to 0.01%: 2 μs

Typical Connection



00555041

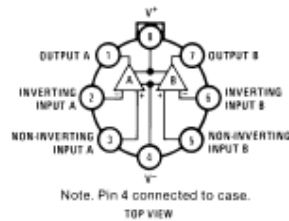
Ordering Information

LF412XYZ

- X indicates electrical grade
- Y indicates temperature range
 - *M" for military
 - *C" for commercial
- Z indicates package type
 - *H" or "N"

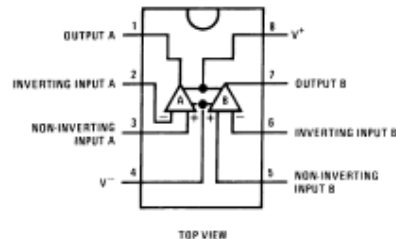
Connection Diagrams

Metal Can Package



Note. Pin 4 connected to case.
TOP VIEW
00555642
Order Number LF412MH, LF412CH
or LF412MH/883 (Note 1)
See NS Package Number H08A

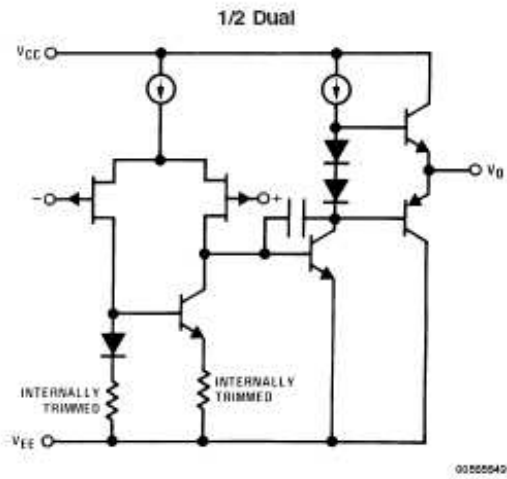
Dual-In-Line Package



TOP VIEW
00555644
Order Number LF412ACN, LF412CN
or LF412MJ/883 (Note 1)
See NS Package Number J08A or N08E

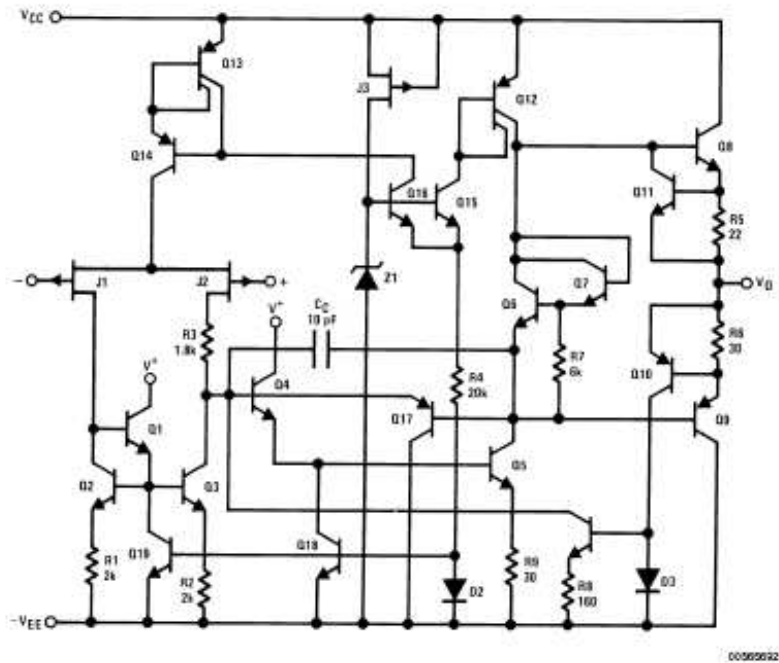
BI-FET II™ is a trademark of National Semiconductor Corporation.

Simplified Schematic



Note 1: Available per JM38510/11905

Detailed Schematic



AC Electrical Characteristics (Continued)

(Note 7)

Symbol	Parameter	Conditions	LF412A			LF412			Units
			Min	Typ	Max	Min	Typ	Max	
THD	Total Harmonic Dist	$A_V=+10$, $R_L=10k$, $V_O=20$ Vp-p, $BW=20$ Hz-20 kHz		≤ 0.02			≤ 0.02		%
e_n	Equivalent Input Noise Voltage	$T_A=25^\circ\text{C}$, $R_S=100\Omega$, $f=1$ kHz		25			25		nV/ $\sqrt{\text{Hz}}$
i_n	Equivalent Input Noise Current	$T_A=25^\circ\text{C}$, $f=1$ kHz		0.01			0.01		pA/ $\sqrt{\text{Hz}}$

Note 3: Unless otherwise specified the absolute maximum negative input voltage is equal to the negative power supply voltage.

Note 4: Any of the amplifier outputs can be shorted to ground indefinitely, however, more than one should not be simultaneously shorted as the maximum junction temperature will be exceeded.

Note 5: For operating at elevated temperature, these devices must be derated based on a thermal resistance of θ_{JA} .

Note 6: These devices are available in both the commercial temperature range $0^\circ\text{C} \leq T_A \leq 70^\circ\text{C}$ and the military temperature range $-55^\circ\text{C} \leq T_A \leq 125^\circ\text{C}$. The temperature range is designated by the position just before the package type in the device number. A "C" indicates the commercial temperature range and an "M" indicates the military temperature range. The military temperature range is available in "H" package only. In all cases the maximum operating temperature is limited by internal junction temperature T_J max.

Note 7: Unless otherwise specified, the specifications apply over the full temperature range and for $V_S=\pm 20\text{V}$ for the LF412A and for $V_S=\pm 15\text{V}$ for the LF412. V_{OS} , I_B , and I_{OS} are measured at $V_{CM}=0$.

Note 8: The LF412A is 100% tested to this specification. The LF412 is sample tested on a per amplifier basis to insure at least 85% of the amplifiers meet this specification.

Note 9: The input bias currents are junction leakage currents which approximately double for every 10°C increase in the junction temperature, T_J . Due to limited production test time, the input bias currents measured are correlated to junction temperature. In normal operation the junction temperature rises above the ambient temperature as a result of internal power dissipation, P_D . $T_J=T_A+\theta_{JA} P_D$ where θ_{JA} is the thermal resistance from junction to ambient. Use of a heat sink is recommended if input bias current is to be kept to a minimum.

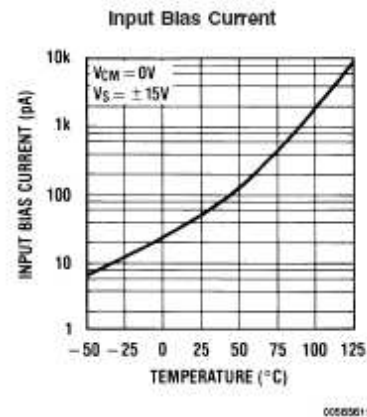
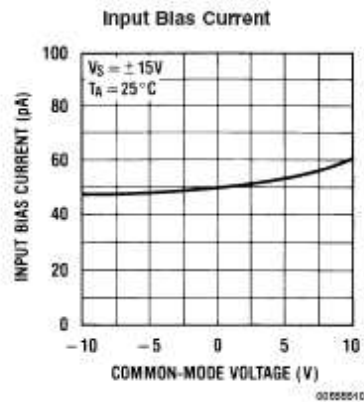
Note 10: Supply voltage rejection ratio is measured for both supply magnitudes increasing or decreasing simultaneously in accordance with common practice. $V_S = \pm 6\text{V}$ to $\pm 15\text{V}$.

Note 11: Refer to PETS412X for LF412MH and LF412MJ military specifications.

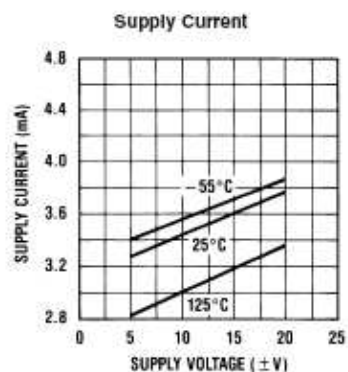
Note 12: Max. Power Dissipation is defined by the package characteristics. Operating the part near the Max. Power Dissipation may cause the part to operate outside guaranteed limits.

Note 13: Human body model, 1.5 k Ω in series with 100 pF.

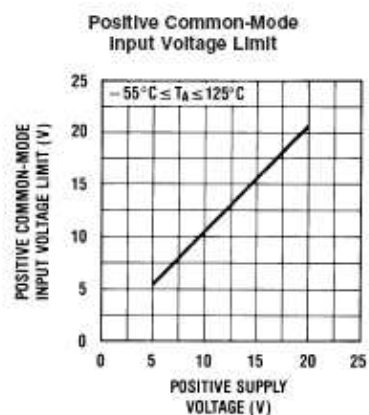
Typical Performance Characteristics



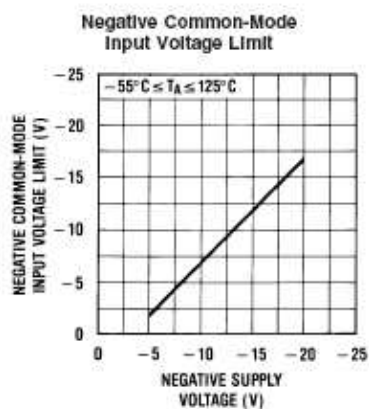
Typical Performance Characteristics (Continued)



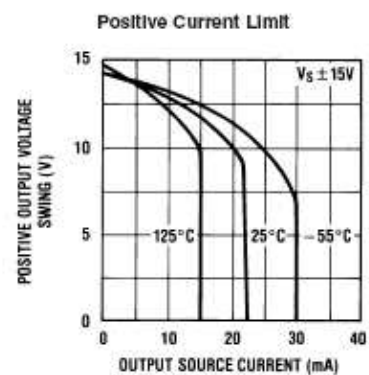
00555612



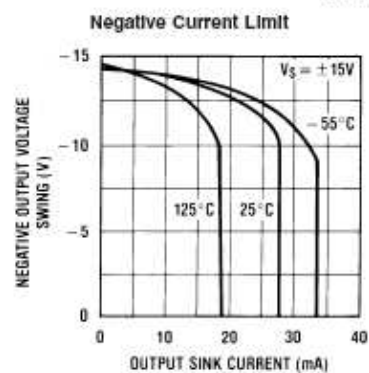
00555613



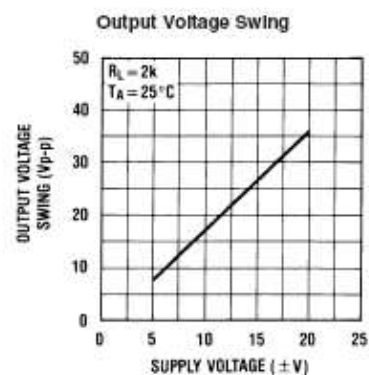
00555614



00555615

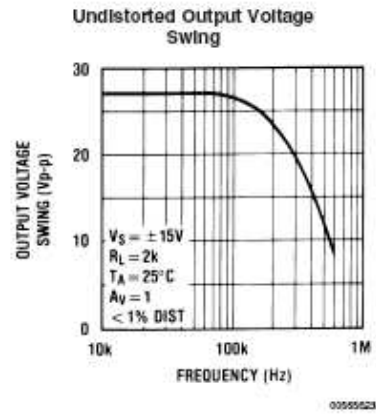
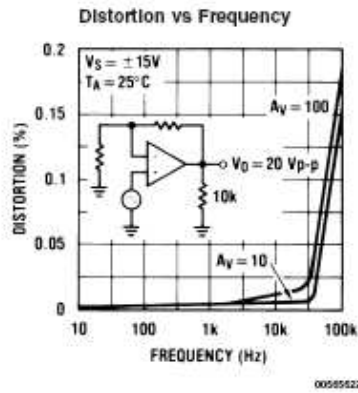
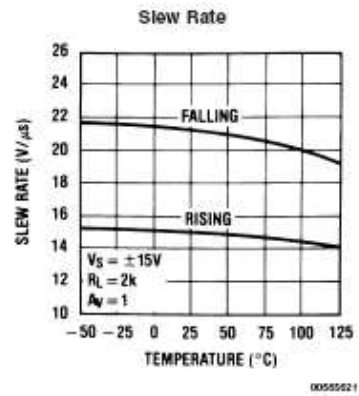
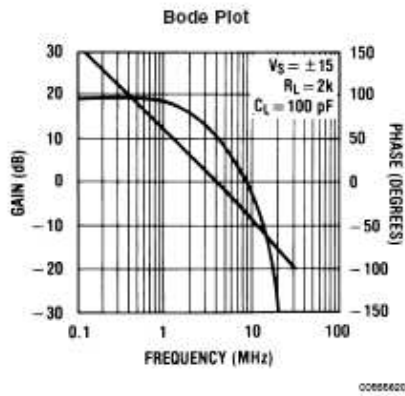
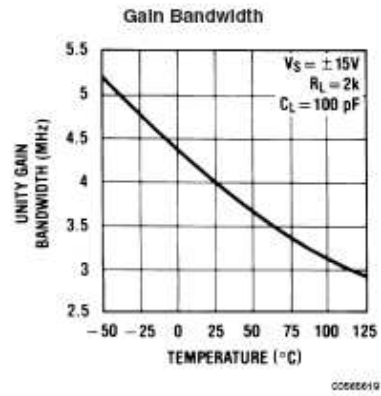
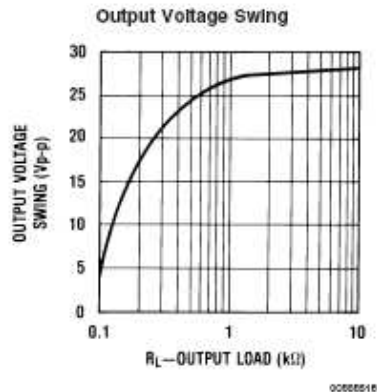


00555616

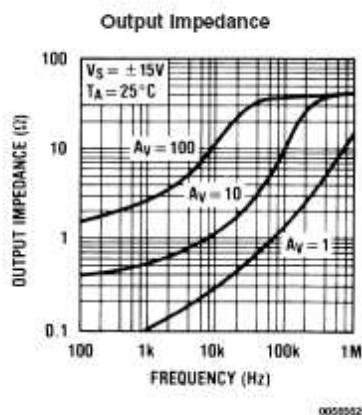
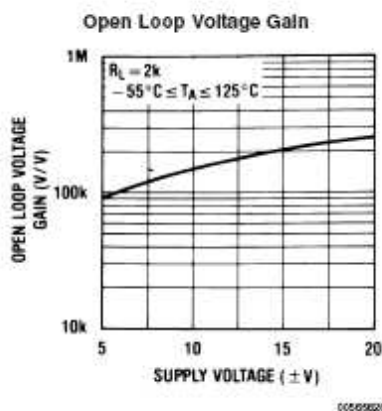
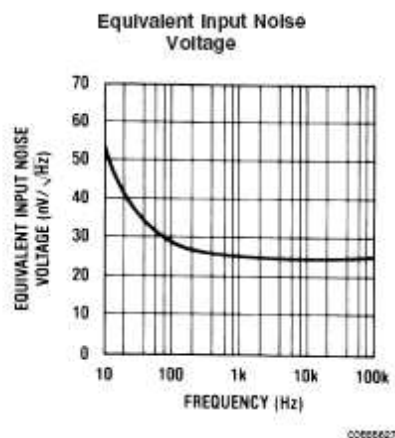
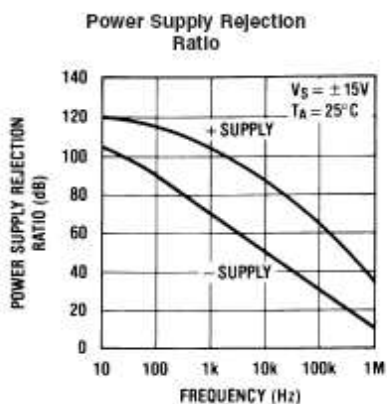
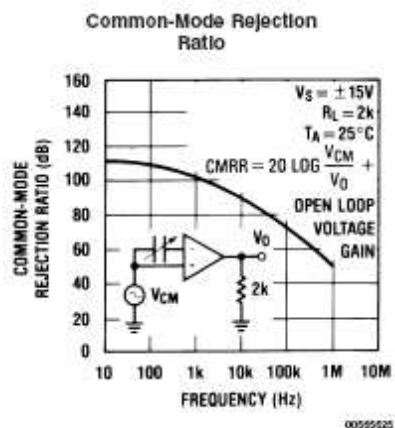
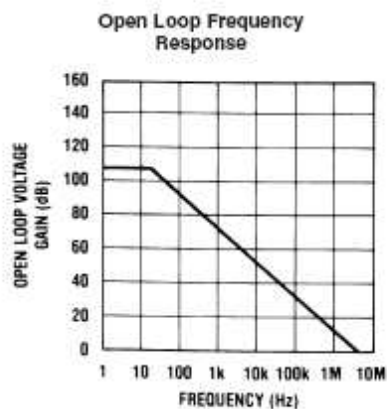


00555617

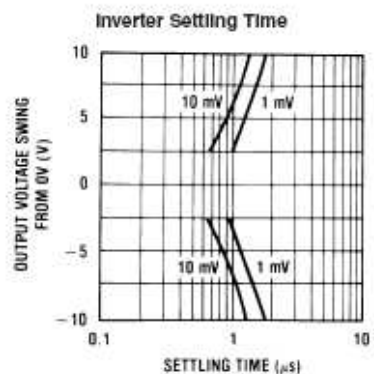
Typical Performance Characteristics (Continued)



Typical Performance Characteristics (Continued)

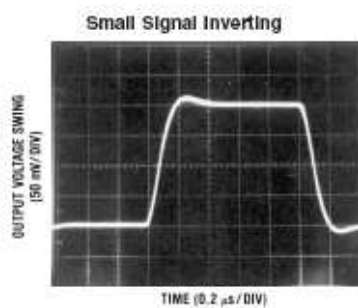


Typical Performance Characteristics (Continued)

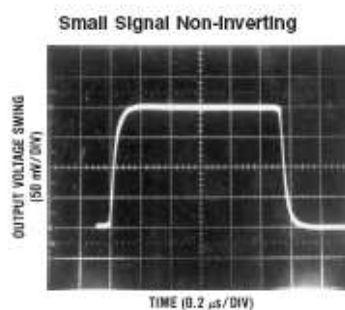


00655520

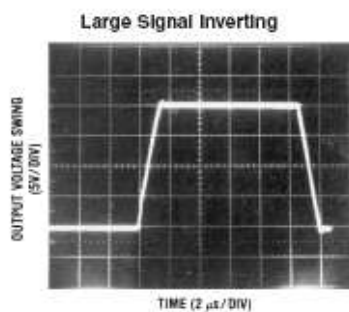
Pulse Response $R_L=2\text{ k}\Omega$, $C_L=10\text{ pF}$



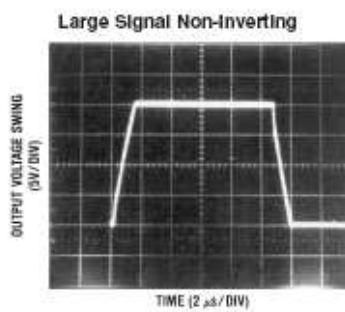
00655530



00655537

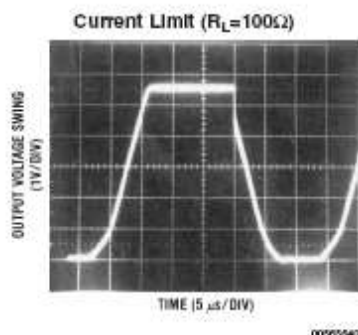


00655538



00655539

Pulse Response $R_L=2\text{ k}\Omega$, $C_L=10\text{ pF}$ (Continued)



Application Hints

The LF412 series of JFET input dual op amps are internally trimmed (BI-FET II™) providing very low input offset voltages and guaranteed input offset voltage drift. These JFETs have large reverse breakdown voltages from gate to source and drain eliminating the need for clamps across the inputs. Therefore, large differential input voltages can easily be accommodated without a large increase in input current. The maximum differential input voltage is independent of the supply voltages. However, neither of the input voltages should be allowed to exceed the negative supply as this will cause large currents to flow which can result in a destroyed unit.

Exceeding the negative common-mode limit on either input will cause a reversal of the phase to the output and force the amplifier output to the corresponding high or low state.

Exceeding the negative common-mode limit on both inputs will force the amplifier output to a high state. In neither case does a latch occur since raising the input back within the common-mode range again puts the input stage and thus the amplifier in a normal operating mode.

Exceeding the positive common-mode limit on a single input will not change the phase of the output, however, if both inputs exceed the limit, the output of the amplifier may be forced to a high state.

The amplifiers will operate with a common-mode input voltage equal to the positive supply; however, the gain bandwidth and slew rate may be decreased in this condition. When the negative common-mode voltage swings to within 3V of the negative supply, an increase in input offset voltage may occur.

Each amplifier is individually biased by a zener reference which allows normal circuit operation on $\pm 6.0\text{V}$ power supplies. Supply voltages less than these may result in lower gain bandwidth and slew rate.

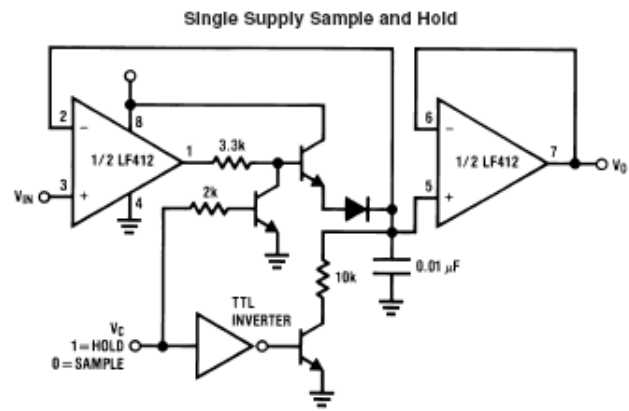
The amplifiers will drive a $2\text{ k}\Omega$ load resistance to $\pm 10\text{V}$ over the full temperature range. If the amplifier is forced to drive heavier load currents, however, an increase in input offset voltage may occur on the negative voltage swing and finally reach an active current limit on both positive and negative swings.

Precautions should be taken to ensure that the power supply for the integrated circuit never becomes reversed in polarity or that the unit is not inadvertently installed backwards in a socket as an unlimited current surge through the resulting forward diode within the IC could cause fusing of the internal conductors and result in a destroyed unit.

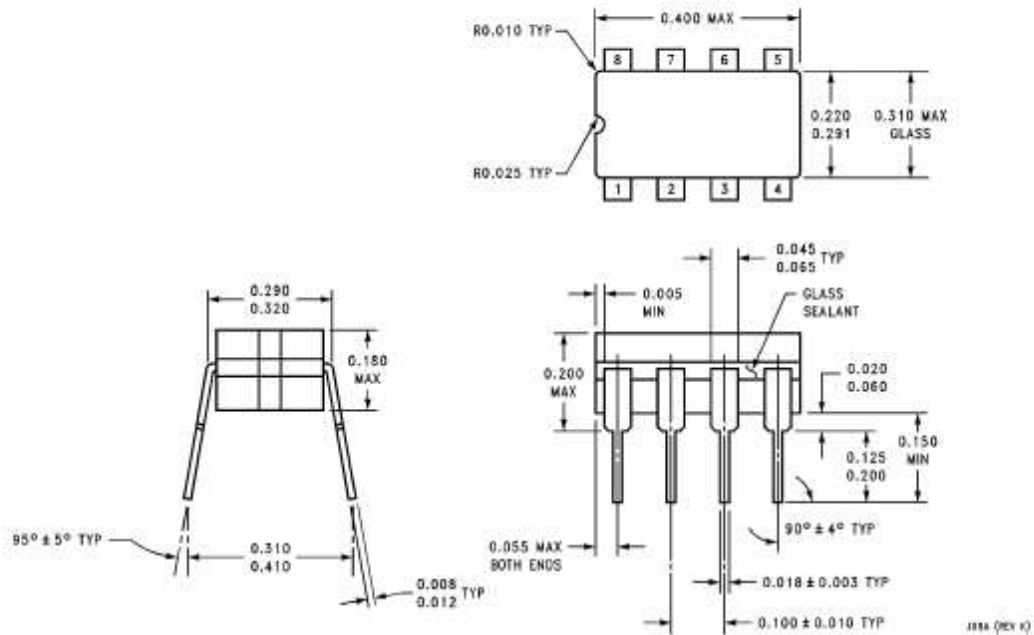
As with most amplifiers, care should be taken with lead dress, component placement and supply decoupling in order to ensure stability. For example, resistors from the output to an input should be placed with the body close to the input to minimize "pick-up" and maximize the frequency of the feedback pole by minimizing the capacitance from the input to ground.

A feedback pole is created when the feedback around any amplifier is resistive. The parallel resistance and capacitance from the input of the device (usually the inverting input) to AC ground set the frequency of the pole. In many instances the frequency of this pole is much greater than the expected 3 dB frequency of the closed loop gain and consequently there is negligible effect on stability margin. However, if the feedback pole is less than approximately 6 times the expected 3 dB frequency a lead capacitor should be placed from the output to the input of the op amp. The value of the added capacitor should be such that the RC time constant of this capacitor and the resistance it parallels is greater than or equal to the original feedback pole time constant.

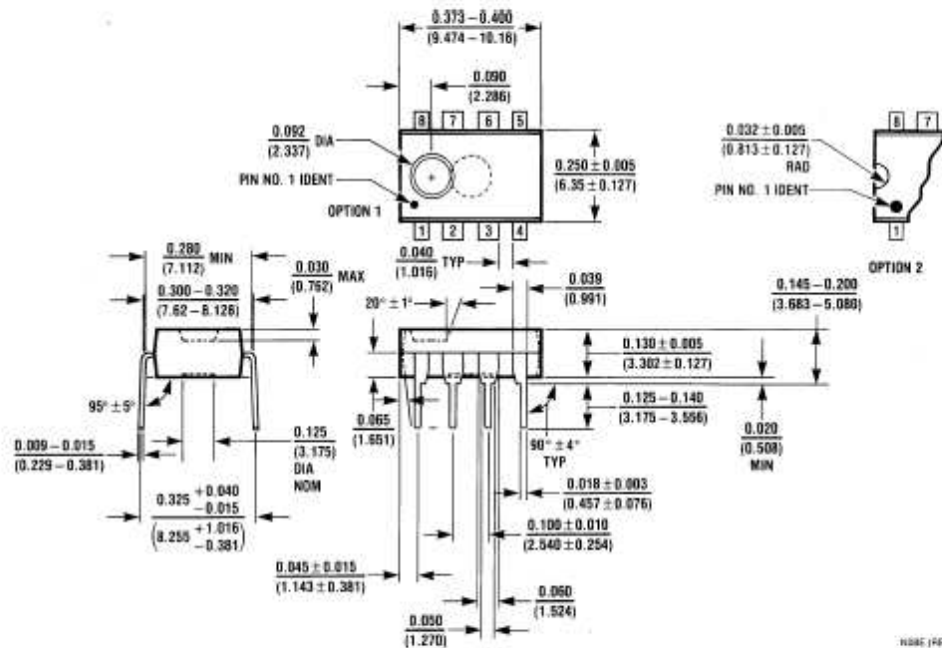
Typical Application



Physical Dimensions inches (millimeters) unless otherwise noted (Continued)



Dual-In-Line Package (J)
Order Number LF412MJ/883
NS Package Number J08A



Dual-In-Line Package (N)
Order Number LF412ACN or LF412CN
NS Package Number N08E

E4: Relevant Syringe Pump User Manual Page

New Era Pump Systems Inc.

www.SyringePump.com

Model NE-1000 Multi-Phaser™

12.7 Syringe Diameters and Rate Limits

Manufacturer	Syringe (cc)	Inside Diameter (mm)	Maximum Rate (mL/hr)	Minimum Rate (µl/hr)
B-D	1	4.699	53.07	0.73
	3	8.585	177.1	2.434
	5	11.99	345.5	4.748
	10	14.43	500.4	6.876
	20	19.05	872.2	11.99
	30	21.59	1120	15.4
	60	26.59	1699	23.35
HSW Norm-Ject	1	4.69	52.86	0.727
	3	9.65	223.8	3.076
	5	12.45	372.5	5.119
	10	15.9	607.6	8.349
	20	20.05	966.2	13.28
	30	22.9	1260	17.32
	50	29.2	2049	28.16
Monoject	1	5.74	79.18	1.088
	3	8.941	192.1	2.64
	6	12.7	387.6	5.326
	12	15.72	593.9	8.161
	20	20.12	972.9	13.37
	35	23.52	1329	18.27
	60	26.64	1705	23.44
Terumo	1	4.7	53.09	0.73
	3	8.95	192.5	2.646
	5	13	406.1	5.581
	10	15.8	600	8.244
	20	20.15	975.8	13.41
	30	23.1	1282	17.63
	60	29.7	2120	29.13
Air-Tite	10	15.9	607.6	8.349
	20	20.25	985.5	13.55
	30	22.5	1216	16.72
	50	29	2021	27.78
	Syringe (µL)	Inside Diameter (mm)	Maximum Rate (µl/hr)	Minimum Rate (µl/hr)
Hamilton Microliter	0.5	0.103	25.49	0.001
	1	0.146	51.23	0.001
	2	0.206	101.9	0.002
	5	0.326	255.4	0.004
SGE	0.5	0.1	24.03	0.001
	1	0.15	54.07	0.001


E5: Infrared LED

LED

Infrared LED L2791 series

Small emission spot LED using current confined chip

L2791 is infrared LED with a microball lens cemented to the current confined chip surface. This combination ensures high directivity and improved emission uniformity. In particular, L2791-02 uses a lens cap that delivers even narrower directivity. As a variant type not using a microball lens, L2791-03 is also available with the LED chip potted with resin, which gives a small emission spot of $\phi 160\ \mu\text{m}$.



Features

- Small emission spot
L2791 : $\phi 400\ \mu\text{m}$
L2791-03: $\phi 160\ \mu\text{m}$
- Uniform emission: L2791/-02
- Narrow directivity: L2791/-02

Applications

- Automatic control systems
- Optical switches
- Auto-focus


■ Absolute maximum ratings (Ta=25 °C)

Parameter	Symbol	Condition	Value	Unit
Forward current	I_F		80	mA
Reverse voltage	V_R		3	V
Pulse forward current	I_{FP}	Pulse width=10 μs Duty ratio=1 %	0.5	A
Operating temperature	T_{opr}		-30 to +85	°C
Storage temperature	T_{stg}		-40 to +100 *	°C

* L2791-03 is guaranteed to resist temperature cycle test of up to 5 cycles.

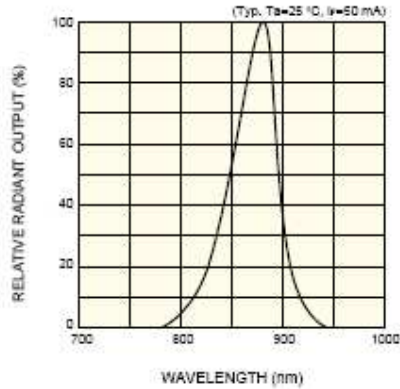
■ Electrical and optical characteristics (Ta=25 °C)

Parameter	Symbol	Condition	L2791			L2791-02			L2791-03			Unit
			Min.	Typ.	Max.	Min.	Typ.	Max.	Min.	Typ.	Max.	
Peak emission wavelength	λ_p	$I_F=50\ \text{mA}$	850	880	910	850	880	910	850	880	910	nm
Spectral half width	$\Delta\lambda$	$I_F=50\ \text{mA}$	-	60	-	-	60	-	-	60	-	nm
Forward voltage	V_F	$I_F=50\ \text{mA}$	-	1.5	1.7	-	1.5	1.7	-	1.5	1.7	V
Pulse forward voltage	V_{FP}	$I_F=0.5\ \text{A}$	-	3.2	4.0	-	3.2	4.0	-	3.2	4.0	V
Reverse current	I_R	$V_R=3\ \text{V}$	-	-	10	-	-	10	-	-	10	μA
Radiant flux	ϕ_e	$I_F=50\ \text{mA}$	1.6	2.0	-	1.6	2.0	-	4.0	5.0	-	mW
Radiant illuminance	P_E	$I_F=50\ \text{mA}$	-	1.3	-	-	2.0	-	-	-	-	mW/cm^2
Rise time	t_r	$I_F=50\ \text{mA}$, 10 to 90 %	-	0.12	0.2	-	0.12	0.2	-	0.12	0.2	μs
Fall time	t_f	$I_F=50\ \text{mA}$, 90 to 10 %	-	0.12	0.2	-	0.12	0.2	-	0.12	0.2	μs



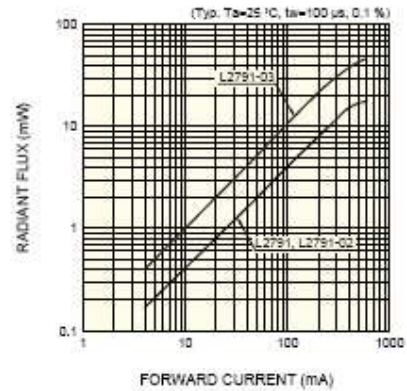
HAMAMATSU

■ Emission spectrum



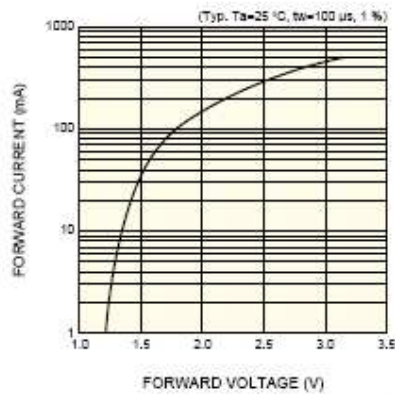
FAJCS001008A

■ Radiant flux vs. forward current



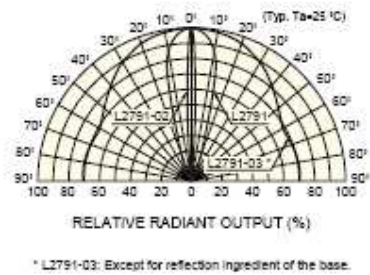
FAJCS001008A

■ Forward current vs. forward voltage



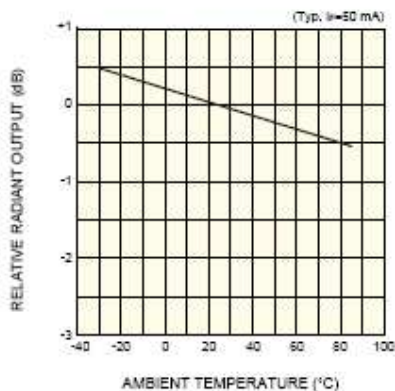
FAJCS001008A

■ Directivity



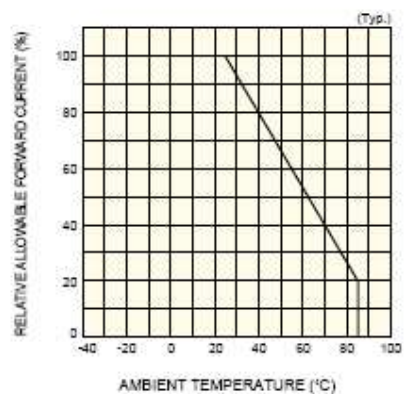
FAJCS001008A

■ Radiant output vs. ambient temperature



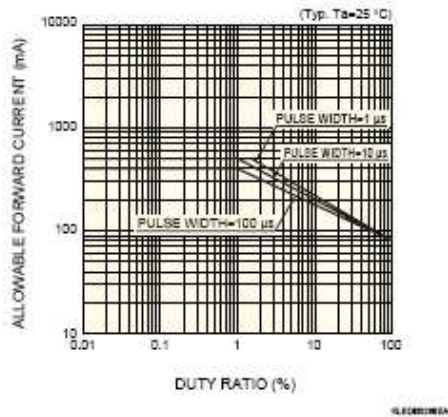
FAJCS001008A

■ Allowable forward current vs. ambient temperature



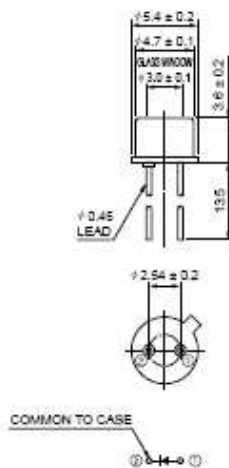
FAJCS001008A

■ Allowable forward current vs. duty ratio

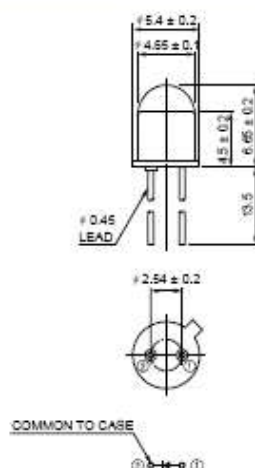


■ Dimensional outlines (unit: mm)

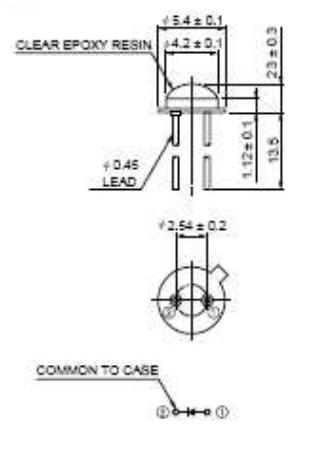
① L2791



② L2791-02



③ L2791-03



HAMAMATSU

Information furnished by HAMAMATSU is believed to be reliable. However, no responsibility is assumed for possible inaccuracies or omissions. Specifications are subject to change without notice. No patent rights are granted to any of the circuits described herein. ©2006 Hamamatsu Photonics K.K.

HAMAMATSU PHOTONICS K.K., Solid State Division

1126-1 Ichino-cho, Hamamatsu City, 435-8556 Japan, Telephone: (81) 053-434-3311, Fax: (81) 053-434-5154, www.hamamatsu.com

U.S.A.: Hamamatsu Corporation, 390 Foothill Road, P.O. Box 6910, Bridgewater, N.J. 08807-0910, U.S.A., Telephone: (1) 908-231-0960, Fax: (1) 908-231-1218

Germany: Hamamatsu Photonics Deutschland GmbH, Azubergstr. 10, D-82211 Herrsching am Ammersee, Germany, Telephone: (49) 08152-3750, Fax: (49) 08152-2858

France: Hamamatsu Photonics France S.A.R.L., 19, Rue du Saule Trépas, Parc du Moulin de Massy, 91862 Massy Cedex, France, Telephone: 33-(1) 69 53 71 00, Fax: 33-(1) 69 53 71 10

United Kingdom: Hamamatsu Photonics UK Limited, 2 Howard Court, 10 Twinn Road, Welwyn Garden City, Hertfordshire AL7 1BW, United Kingdom, Telephone: (44) 1707-294888, Fax: (44) 1707-325777

North Europe: Hamamatsu Photonics Norden AB, Smålandsgatan 12, SE-171 41 Solna, Sweden, Telephone: (46) 8-550-031-00, Fax: (46) 8-550-031-01

Italy: Hamamatsu Photonics Italia S.R.L., Strada della Mole, 1/E, 20020 Avese, (Milano), Italy, Telephone: (39) 02-935-81-733, Fax: (39) 02-935-81-741

Cat. No. KLED1021E02
Jun. 2006 DN 3

ACKNOWLEDGMENTS

We would like to thank Dr. Kevin Lear PhD for his help and guidance, as well as four of his graduate students, Bob Pownall, Hua (Linda) Shao, Sean Pieper and Weina Wang, for all of their help.